Bioconjugate Chemistry

Editors' Choice
Open Access

pubs.acs.org/bc

Article

NanoBondy Reaction through NeissLock Anhydride Allows Covalent Immune Cell Decoration

Lasya R. Vankayala, Kish R. Adoni, Sheryl Y. T. Lim, Tommy Dam, Omer Dushek, Konstantinos Thalassinos, and Mark R. Howarth*

Cite This: https://doi.org/10.1021/acs.bioconjchem.5c00519

Read Online

ACCESS | Metrics & More | Article Recommendations | Supporting Information

ABSTRACT: Cell-surface conjugation has enormous therapeutic and research potential. Existing technologies for cell-surface modification are usually reversible, nonspecific, or rely on genetic editing of target cells. Here, we present the NanoBondy, a nanobody modified for covalent ligation to an unmodified protein target at the cell surface. The NanoBondy utilizes the 20 naturally occurring amino acids, harnessing NeissLock chemistry engineered from *Neisseria meningitidis*. We evaluated the binding and specificity of a panel of nanobodies to CD45, a long-lived surface marker of nucleated hematopoietic cells. We demonstrated the conversion of existing nanobodies to covalently reacting NanoBondies using a disulfide clamp to position the self-processing module of FrpA close to the nanobody antigen-binding site. The addition of calcium induces anhydride formation at the NanoBondy C-terminus, enabling proximity-directed ligation to surface amines on CD45. We optimized the NanoBondy reaction by fine-tuning linkers and disulfide clamp sites to modulate anhydride positioning. Tandem mass spectrometry mapped reaction sites between NanoBondy and CD45. NanoBondy ligation was robust to buffer, pH, and temperature and was detected within 2 minutes. We established the reaction specificity of NanoBondies to endogenous CD45 at the surface of NK cells and T cells. NanoBondy technology provides a modular approach for targeted, inducible, and covalent cell-surface modification of immune cells without their genetic modification.

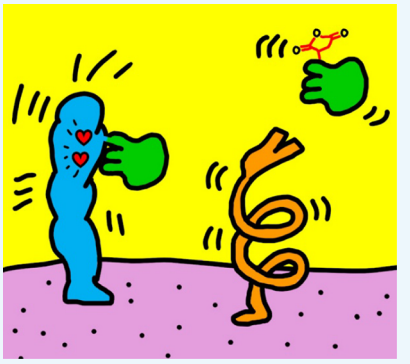

INTRODUCTION

Molecular recognition in living systems is dominated by networks of noncovalent contacts. However, many applications in research and biotechnology are limited by the instability of such binding interactions.[1,2] Instability may pose a challenge in response to harsh conditions or force, but it is most commonly an issue for long-lasting labeling, such as when attempting to change cell behavior *in vivo*.[3,4] There has been particular excitement about cell-surface conjugation to enhance cell therapy, given the great success of chimeric antigen receptor (CAR)-T cells against leukemia and lymphoma.[5−7] However, CAR-T cells have not yet fulfilled their potential in destroying solid tumors.[5−7] To enhance therapeutic activity, T cells have been armed with cytokines, small molecule drugs, checkpoint inhibitors, or extracellular matrix-degrading enzymes, either directly[8−10] or within nanoparticles[11−15] or nanogels.[16]

Modular tags for covalent ligation (e.g., HaloTag,[17] SNAP-tag,[18] SpyTag/SpyCatcher,[19] split intein,[20] sortase[21]) have been valuable for cell-surface decoration.[22−24] However, in cell therapy, the bacterial origin of most tag systems may raise immunogenicity concerns.[24,25] Genetic modification of cell therapies also faces challenges, including the time required from transduction to surface expression, the potential for insertional mutagenesis, and innate immune activation caused by nucleic acid delivery.[26] Each genetic change to cells adds to the delay, complexity, and cost of this exceptionally expensive therapeutic class.[27] Cells may also be modified by inserting hydrophobic moieties into the plasma membrane, which is widely applicable but lacks specificity of insertion site or cell type.[28,29] In addition, the hydrophobic tails gradually deinsert from the plasma membrane and can reinsert into neighboring cells.[30] Covalent ligation has been achieved through metabolic labeling using amino acids or carbohydrates with bio-orthogonal groups, which leads to surface display for click reactions.[13,31−33] Chemical cross-linkers[11,14,15] or N-hydroxysuccinimide-based biotinylation followed by streptavidin labeling also allow stable cell decoration.[34] However, such approaches modify multiple proteins, which may interfere with cell function.[4,35]

Nanobodies, also known as Variable Heavy domain of Heavy chain (VHH) or single-domain antibodies (sdAb), are a binding scaffold typically derived from immunizing llamas, alpacas, or camels. Nanobodies are an excellent platform for

Received: October 20, 2025
Revised: December 1, 2025
Accepted: December 15, 2025

molecular engineering, given their small size, stability, high affinity, and ease of production in *Escherichia coli*.[36,37] Unnatural amino acid mutagenesis has been used to generate covalently reactive nanobodies for the Sulfur Fluoride Exchange (SuFEx) reaction[31,32] or the singlet oxygen-induced reaction of a furan warhead,[38] but it faces challenges in scalability toward large-scale protein production.[39] To create a new modality for covalent recognition of unmodified proteins, here we describe the NanoBondy, a covalently reactive nanobody harnessing our group's NeissLock chemistry.[40] NeissLock is engineered from the self-processing module (SPM) of FrpA[41] of *Neisseria meningitidis*. Addition of calcium activates SPM, resulting in rapid autoproteolysis at an aspartate-proline bond. This step leads to formation of a highly electrophilic anhydride,[40,42] which then can undergo attack by water or by nucleophiles such as amines on nearby proteins (Figure 1A). While the NeissLock SPM module is bacterially derived, calcium addition results in the release of the SPM moiety. As a result, the final conjugated adduct contains only a single amino acid scar: the Asp derived from the N-terminus of SPM. NeissLock has previously been used to lock together preexisting protein−protein interactions that are naturally present in a specific organism, where there is a high-resolution structure of the complex in the Protein Data Bank (PDB).[40] Here, we advance NeissLock technology beyond endogenously occurring protein−protein pairs to artificial complexes where there is no experimental structure. By engineering the fusion of this SPM to a preexisting nanobody, with precise linkers and a disulfide clamp, we enable covalent conjugation of a nanobody to its protein target in an inducible and targeted manner, after which the SPM moiety can diffuse away (Figure 1B). We optimize NanoBondy conjugation in the context of the cell-surface target CD45, which is a long-lived and broadly expressed immune marker.[43] We determine key features of the NanoBondy design for anhydride positioning and establish its robustness to reaction conditions for coupling to the isolated glycosylated extracellular domain. We then validate the NanoBondy coupling speed and specificity on cell lines and primary human immune cells. Extending the NanoBondy system, we then construct a DuoBondy, capable of covalent attachment to CD45, while including a second binder moiety allowing noncovalent attachment to the cancer checkpoint inhibitor target PD-1.

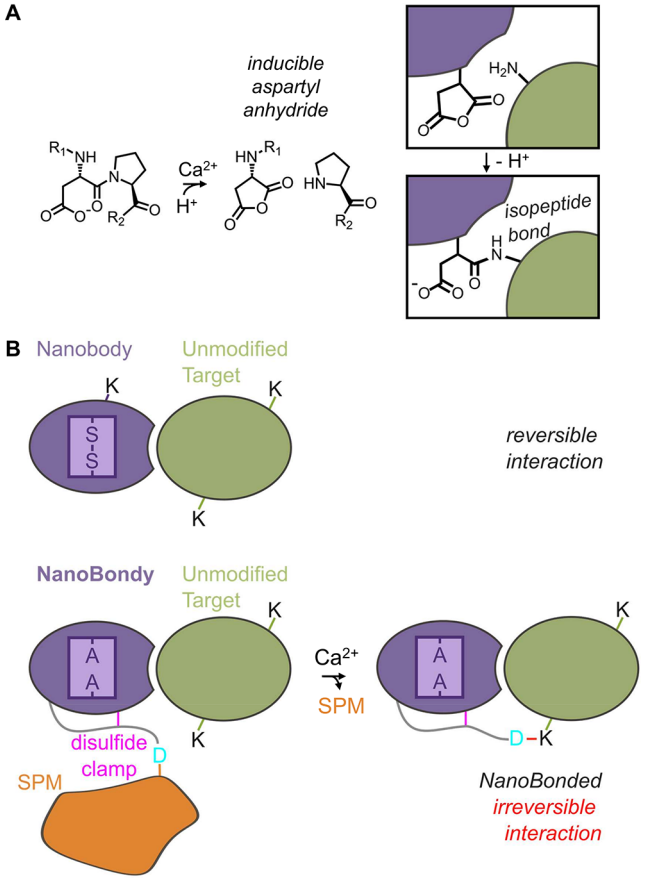

Figure 1. NanoBondy principle. (A) NeissLock chemistry. Upon the addition of calcium, the self-processing module (SPM) activates autoproteolysis at the aspartate−proline bond. This step generates a highly reactive aspartyl anhydride, which undergoes nucleophilic attack by a nearby nucleophilic amino acid or water. Fusing SPM to a binder (purple) thereby allows inducible covalent coupling to a target protein (green). (B) NanoBondy design. A nanobody (purple) employs complementarity-determining regions (CDRs) close to the N-terminus to bind its target (green). A regular nanobody can be engineered into a covalently reacting NanoBondy by inclusion of a flexible linker and disulfide clamp (magenta) to hold the reactive D (cyan) of SPM (orange) near the target, allowing anhydride-mediated covalent conjugation to the target after calcium activation.

RESULTS

Selected Nanobody Candidates Demonstrate Specific Binding to CD45

Nanobodies to CD45 were previously generated from llama immunization.[44] We selected 5 nanobodies that bind the d1d2 region of human CD45, furthest from the plasma membrane and conserved across isoforms of CD45.[44] We cloned these nanobodies for bacterial expression with a C-terminal SpyTag003.[45] All five nanobodies were solubly expressed in *E. coli* and were efficiently purified using SpySwitch affinity chromatography[46] (Figure 2A).

We expressed a recombinant fragment of the d1 and d2 domains of human CD45 (Figure 2B) linked to an AviTag for site-specific biotinylation (CD45d1d2) in Expi293F cells. Nanobody binding to CD45d1d2 was evaluated by an enzyme-linked immunosorbent assay (ELISA). All nanobodies demonstrated high-affinity binding to CD45d1d2, with 2H5 demonstrating the best affinity (Figure 2C). The negative control anti-HER2 nanobody showed negligible background binding to CD45d1d2 (Figure 2C).

Nanobody binding to endogenous human CD45 at the cell surface was tested by flow cytometry. Nanobodies were incubated with the YTS and NK92 natural killer (NK) cell lines (each $CD45^+$), using Expi293F cells ($CD45^-$) as a negative control. All nanobodies demonstrated binding to both $CD45^+$ NK cell lines, with minimal nonspecific binding to $CD45^-$ cells (Figure 2D). The anti-HER2 nanobody served as a positive control, and the $HER2^+$ Expi293F cells could be stained successfully (Figure 2D). For further NanoBondy development, we prioritized 2H5 as the highest-affinity binder based on ELISA, as well as high-level and specific staining in flow cytometry.

Designed NanoBondies Demonstrate Specific, Inducible Coupling to Purified CD45

In the absence of experimental structures for complexes with these nanobody binders, we utilized AlphaFold2-multimer[47,48]

https://doi.org/10.1021/acs.bioconjchem.5c00519
Bioconjugate Chem. XXXX, XXX, XXX−XXX

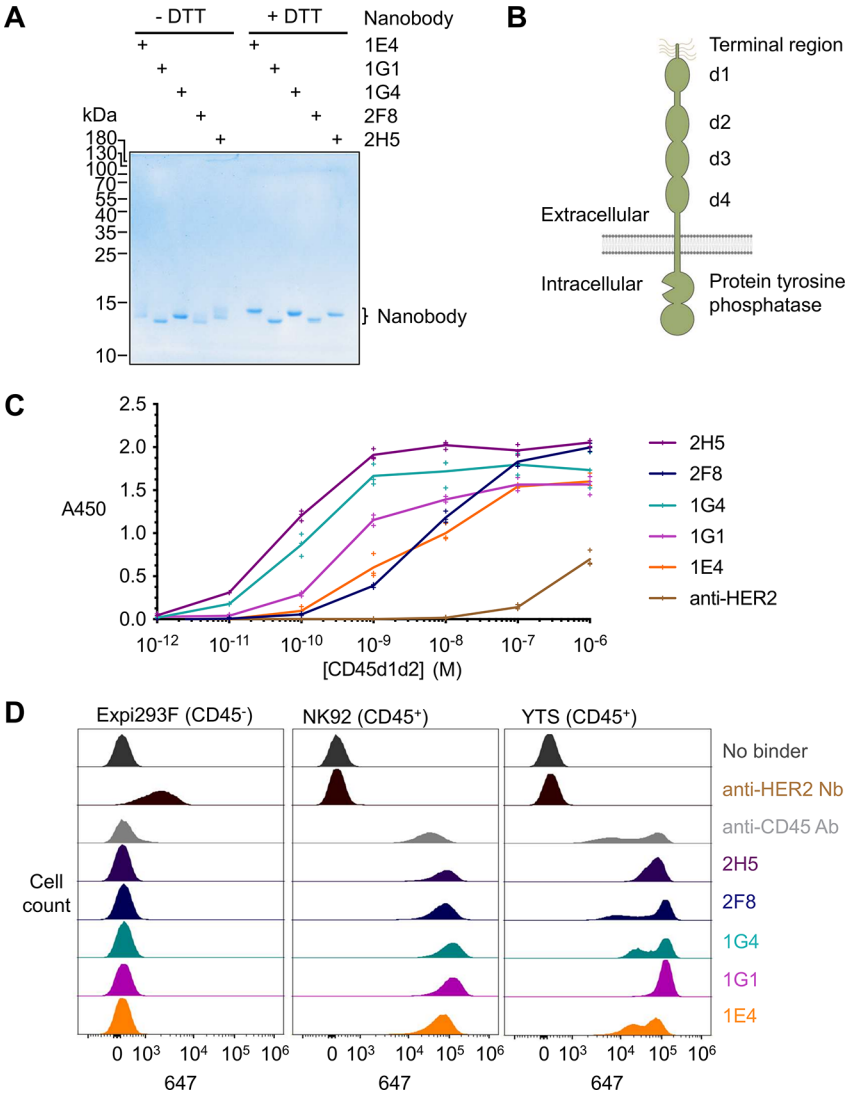

Figure 2. Characterization of anti-CD45 nanobodies. (A) Purification of anti-CD45 nanobodies. Nanobodies were expressed in *E. coli* and purified by SpySwitch affinity chromatography, followed by SDS-PAGE ± dithiothreitol (DTT) and Coomassie staining to assess disulfide bond formation. The experiment was conducted once. (B) Schematic of the organization of CD45, including extracellular domains d1−d4. (C) Binding of nanobodies to purified CD45. Nanobodies were coated on a plate and incubated with the indicated concentration of biotinylated human CD45 domains 1 and 2 (CD45d1d2), followed by colorimetric ELISA detection (absorbance at 450 nm). Anti-HER2 nanobody was used as a negative control. Each triplicate data point is shown with a line connecting the mean. Representative ELISA data were obtained from two independent experiments. (D) Binding of anti-CD45 nanobodies at the cell surface by flow cytometry. Anti-CD45 nanobodies were incubated with Expi293F, NK92, or YTS cells. Nanobody binding was detected using anti-VHH-Alexa Fluor 647. Anti-CD45 antibody was used as a positive control, with anti-HER2 nanobodies or unstained (no binder) cells as negative controls. Representative flow cytometry data were obtained from two independent experiments for Expi293F and YTS and one experiment with all three cell lines.

and ParaFold[49] to predict docking of a 2H5-derived NanoBondy to CD45d1d2 (Figure 3A). A NanoBondy is generated by fusing FrpA SPM to the nanobody's C-terminus via a flexible linker containing a cysteine clamp to position the C-terminal anhydride of the NanoBondy close to the target for reaction (Figure 1B). Before the Asp-Pro cleavage site, we place a Gly-Ser-Tyr linker, which we previously established as optimal for rapid, high-yielding cleavage and anhydride generation.[40]

Based on the AlphaFold model, R72C on the nanobody was identified as the initial site for the disulfide clamp. Two endogenous cysteines in the nanobody, which form the core disulfide bond, were mutated to alanine to minimize any potential disulfide mispairing (Figure 1B). The designed NanoBondy (amino acid sequence in Figure S1) was expressed solubly in *E. coli* and purified using either C-tag or Ni-NTA purification. This NanoBondy was further validated by intact protein electrospray ionization mass spectrometry (Figure S2).

To allow simpler discrimination of reactant and product bands in gel assays, we cloned CD45d, which consists of CD45d1d2 with the maltose-binding protein (MBP) fused at its C-terminus. CD45d expresses well in Expi293F cells, yielding 88 mg per liter of culture (Figure 3B). Both CD45d1d2 and CD45d exhibit extensive N-linked glycosylation. We showed that Peptide:N-Glycosidase F (PNGase F) digestion facilitated analysis by SDS-PAGE (Figure 3B).

To test the 2H5 R72C NanoBondy reactivity to CD45d, the NanoBondy was mixed with CD45d or irrelevant protein targets in equimolar concentrations. We induced conjugation for 1 h at 37 °C with 2 mM $CaCl_2$, comparable in

https://doi.org/10.1021/acs.bioconjchem.5c00519
Bioconjugate Chem. XXXX, XXX, XXX−XXX

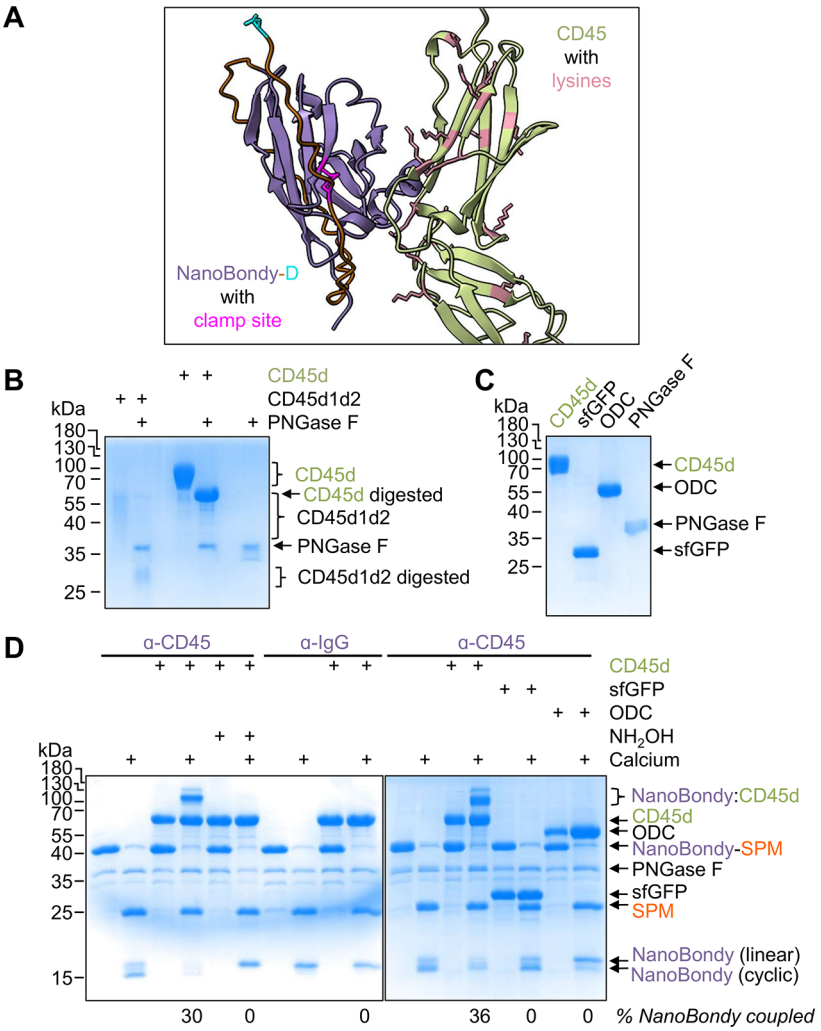

Figure 3. NanoBondy covalent conjugation to recombinant CD45. (A) AlphaFold prediction of 2H5 nanobody (purple) interaction with CD45d1d2 (green). Magenta represents the site for a disulfide clamp, with lysines on CD45d1d2 colored pink and the terminal aspartate in cyan. (B) MBP fusion improved the CD45 gel-based analysis. CD45d consists of MBP fused to domains 1 and 2 of CD45. PNGase F digestion decreased heterogeneous mobility of CD45d1d2 and CD45d upon SDS-PAGE with Coomassie staining. (C) Individual protein components for the conjugation assay in (D). CD45d, sfGFP, ODC, and PNGase F were validated by SDS-PAGE/Coomassie staining. (D) Specificity of the NanoBondy reaction with recombinant CD45. Anti-CD45 2H5 R72C or anti-IgG NanoBondy-SPM was incubated with CD45d, each at 10.5 μM, for 1 h at 37 °C in HBS ± calcium, followed by SDS-PAGE with Coomassie staining. ODC, sfGFP, and anti-IgG NanoBondy were used as negative controls for reaction specificity. Hydroxylamine was used as a competing nucleophile to block reactivity. Colon represents a covalent conjugate. The experiment was conducted once.

concentration to the extracellular medium.[50] The NanoBondy demonstrated calcium-inducible covalent conjugation to CD45d, which was competed out by the strong nucleophile hydroxylamine (NH_2OH) (Figure 3D). We have previously shown that hydroxylamine quenches the SPM-derived anhydride.[40] We generated a negative control NanoBondy by fusion of SPM to the anti-IgG nanobody TP1170. Covalent conjugation showed specificity for the anti-CD45 NanoBondy, with no product band observed when the anti-IgG NanoBondy was mixed with CD45d in the presence of calcium (Figure 3D). The anti-CD45 NanoBondy did not show conjugation to the noncognate protein targets superfolder GFP (sfGFP, expected NanoBondy covalent product mass of 44.5 kDa) or ornithine decarboxylase (ODC, expected NanoBondy covalent product mass of 70.6 kDa) (Figure 3C,D). We also showed the generality of converting different nanobodies to NanoBondies, demonstrating the specificity of coupling to CD45d by a NanoBondy based on a separate anti-CD45 nanobody, 2F8 (Figure S3).

The NanoBondy Clamp Site and Linker Length Alter Conjugation Yield

We tested 3 alternative clamp sites in our NanoBondy design (Figure 4A), with clamp sites arranged in a tripod-like format, so that the resultant anhydride could sample various surfaces on the target. The reaction of NanoBondy with CD45d at different sites yielded different reaction bands that were resolved by SDS-PAGE. The abundance of each reaction band was altered by the choice of clamp site, with R72C demonstrating the highest reaction efficiency (Figure 4B), as evaluated by gel densitometry.

We then varied the length of the flexible linker between the cysteine clamp site and the start of the SPM, testing lengths from 3 to 18 residues, to allow the anhydride to access more distant nucleophilic sites on the target. Interestingly, Nano-

https://doi.org/10.1021/acs.bioconjchem.5c00519
Bioconjugate Chem. XXXX, XXX, XXX−XXX

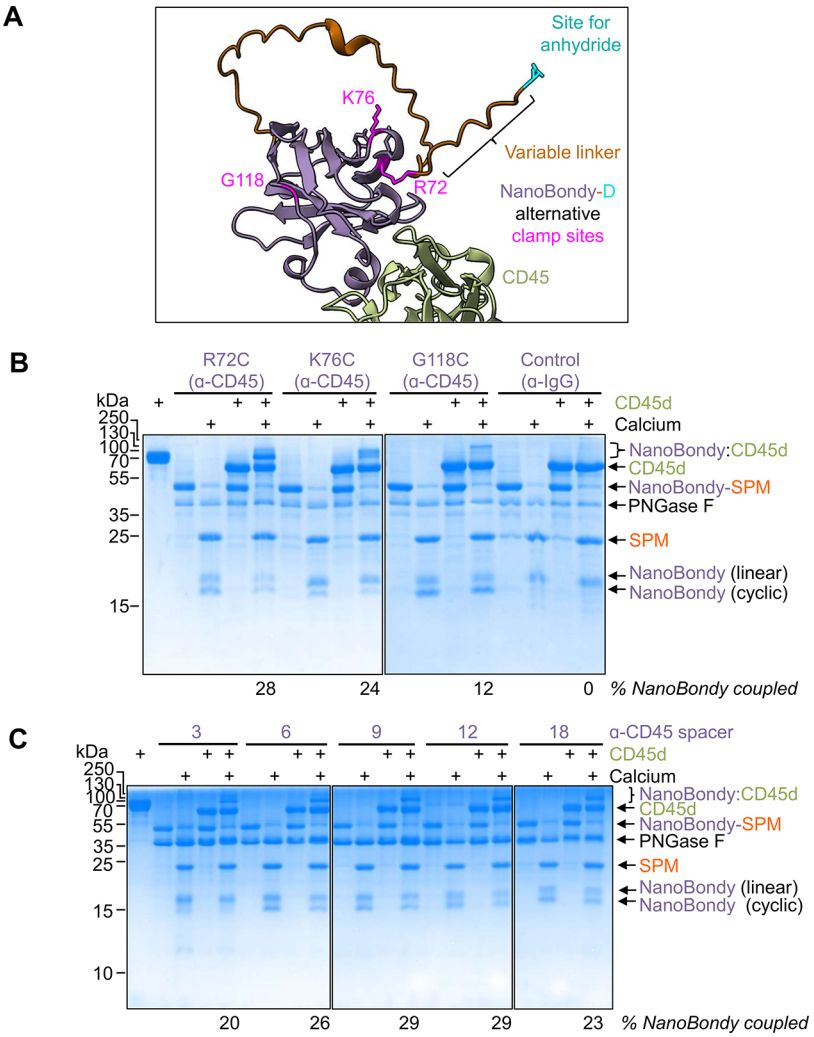

Figure 4. Optimization of NanoBody clamp site and linker length. (A) AlphaFold prediction of 2H5 NanoBody (purple) bound to CD45d1d2 (green). The reactive anhydride is shown in cyan, alternative clamp sites are shown in magenta, and linkers are shown in orange. (B) Clamp-site variant reactivity. 2H5 NanoBody variants were incubated with CD45d at 10.5 μM each for 1 h at 37 °C in HBS ± Ca^{2+}, followed by SDS-PAGE with Coomassie staining. Anti-IgG NanoBody was used as a negative control. The leftmost lane represents CD45d without PNGase F treatment. The experiment was conducted once. (C) Linker variant reactivity for 2H5 R72C anti-CD45 NanoBody, analyzed as in (B). Representative gels were obtained from two independent experiments.

Bondy coupling to the CD45d target was still efficient despite these large changes in linker length (Figure 4C). By gel densitometry, we determined that the overall conjugation yield decreased when 3- and 6-residue linkers were employed. Increasing the linker length beyond 9 residues, however, did not improve conjugation efficiency. From these analyses, we selected the clamp site R72C and a 9-residue linker for further exploration.

The NanoBondy Retains Reactivity across Various Conditions

Next, we evaluated the condition-dependence of the NanoBondy reaction, testing covalent conjugation to its target under various situations involving buffer, temperature, and pH. The NanoBondy was incubated with CD45d in the presence of calcium for varying durations before analysis by SDS-PAGE/Coomassie. The conjugation product was visible within 2 min under most conditions. The reaction proceeded more efficiently in HEPES Buffered Saline (HBS) than Tris-Buffered Saline (TBS) (Figure 5A). The reaction was faster at 37 °C than at 25 °C, with the majority of conjugation completed within 5 min at 37 °C (Figure 5A). We also evaluated pH-dependence by conducting the reaction in HBS along with 2-(N-morpholino)ethanesulfonic acid (MES), which enables effective buffering over a wider pH range. NanoBondy reactivity was retained at pH 6.5−8.5, but the reaction proceeded more slowly at pH 8.5 than at pH 6.5 or 7.5 (Figure 5B). From these analyses, the optimal buffer conditions for the NanoBondy reaction are HBS at 37 °C and pH 7.5. Phosphate Buffered Saline (PBS) is not advised for NanoBondy reactions: the addition of calcium to activate the reaction would result in calcium phosphate precipitation.

Cross-Linking MS/MS Identifies Sites of NanoBondy-CD45d Cross-Linking

To identify the site of NanoBondy cross-linking to CD45d, the 2H5 R72C anti-CD45 NanoBondy and CD45d were mixed at 10.5 μM each in HBS, for a total protein content of 1 mg per reaction, before the addition of calcium. The cross-linked proteins were separated by high pH reverse-phase separation, and the fractions were analyzed by cross-linking tandem mass spectrometry (CL-MS/MS) to identify the dominant reaction

https://doi.org/10.1021/acs.bioconjchem.5c00519
Bioconjugate Chem. XXXX, XXX, XXX−XXX

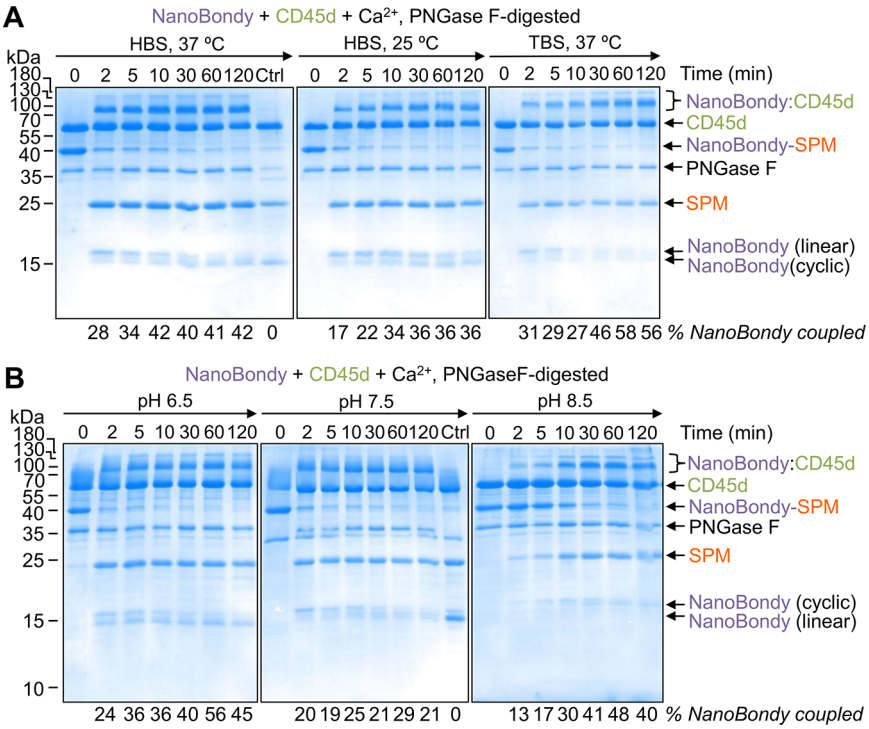

Figure 5. Condition-dependence of NanoBondy reaction. (A) Buffer- and temperature-dependence of NanoBondy reaction. 2H5 R72C anti-CD45 NanoBondy was incubated with CD45d, each at 10.5 μM, in the indicated buffer and temperature before SDS-PAGE with Coomassie staining. Ctrl refers to the lane containing anti-IgG NanoBondy with CD45d for 120 min. Representative gel from two independent experiments. (B) pH-dependence of NanoBondy reaction. The reaction was evaluated as in (A) with HBS-MES buffer at the indicated pH at 37 °C. Ctrl refers to the lane containing anti-IgG NanoBondy with CD45d for 120 min. The experiment was conducted once.

sites (Figure 6). Cross-linking MS/MS indicated that the NanoBondy aspartyl anhydride formed covalent bonds predominantly to 4 different lysines on CD45d (Figures 6A/B and S4). The cross-linked lysines were all located near the AlphaFold-predicted interface, consistent with the structure prediction (Figure 6C).

To further investigate these predictions, we generated point mutations of CD45d at the predicted interface with NanoBondy (Figure S5A). The single mutants of CD45d, I104R or E105R, expressed well in Expi293F cells but caused a substantial loss in both covalent coupling by the anti-CD45 NanoBondy (Figure S5B) and noncovalent docking, as tested by ELISA (Figure S5C). These mutational experiments further validated the AlphaFold-predicted interface.

Cross-linking MS/MS identified a single own-goal site, where the NanoBondy anhydride formed an ester bond with Ser56 on the NanoBondy itself (Figure 6A/B, S4D). This is the first time that NeissLock has demonstrated covalent reaction with a serine.[40] We have previously shown that the SPM anhydride is reactive to nucleophiles resembling the side chains of cysteine and tyrosine, as well as to α-amines, such as those at the protein N-terminus.[40] The anti-CD45 NanoBondy contains two cysteine residues and 13 tyrosine residues. CD45d contains ten cysteine residues and six tyrosine residues. However, we did not observe NanoBondy-mediated conjugation to cysteine, tyrosine, or the α-amino group on either CD45d or the NanoBondy itself.

NanoBondy Demonstrates Targeted Covalent Coupling at the Cell Surface

To test the NanoBondy's reaction to CD45 at the cell surface, we initially used YTS, a human NK cell line. Cells were incubated with NanoBondy in the presence of 2 mM $CaCl_2$ for 1 h at 37 °C. We evaluated NanoBondy reactivity to the YTS cell surface via Western blotting. When blotting for the nanobody moiety (VHH), we consistently observed a high molecular weight band following calcium addition, corresponding to the reaction product between NanoBondy and CD45. CD45RO migrates at 180 kDa.[51,52] Therefore, the mass of the NanoBondy:CD45 conjugate would have an expected molecular weight of approximately 198 kDa. The observed covalent conjugate band migrated between the 185 and 270 kDa markers. We did not observe nonspecific bands, indicating that NanoBondy reaction is targeted to CD45 without promiscuous reactivity to diverse cell surface proteins (Figure 7A).

Conjugation was blocked upon the addition of hydroxylamine, indicating that the observed product depends on anhydride-mediated reactivity. At 5 μM NanoBondy, we did not observe conjugation of the irrelevant NanoBondy control to $CD45^+$ cells or conjugation of the anti-CD45 NanoBondy to the $CD45^-$ Expi293F cells (Figure 7A). When blotting for CD45, we observed that the CD45 band demonstrated an upward shift upon NanoBondy reaction (Figure 7B), supporting that the NanoBondy is reacting with endogenous CD45 at the cell surface. To further test the cell-surface staining by the anti-CD45 NanoBondy, we incubated human primary $CD8^+$ T cells ($CD45^+$) or Expi293F cells ($CD45^-$) and visualized cell-surface staining using live-cell confocal microscopy (Figure S8). Surface staining by the anti-CD45 NanoBondy was detected only on the $CD8^+$ T cells.

To establish NanoBondy technology for covalent delivery of effector proteins, we generated a DuoBondy consisting of an anti-PD-1 nanobody[53] attached N-terminally to the covalently

https://doi.org/10.1021/acs.bioconjchem.5c00519
Bioconjugate Chem. XXXX, XXX, XXX−XXX

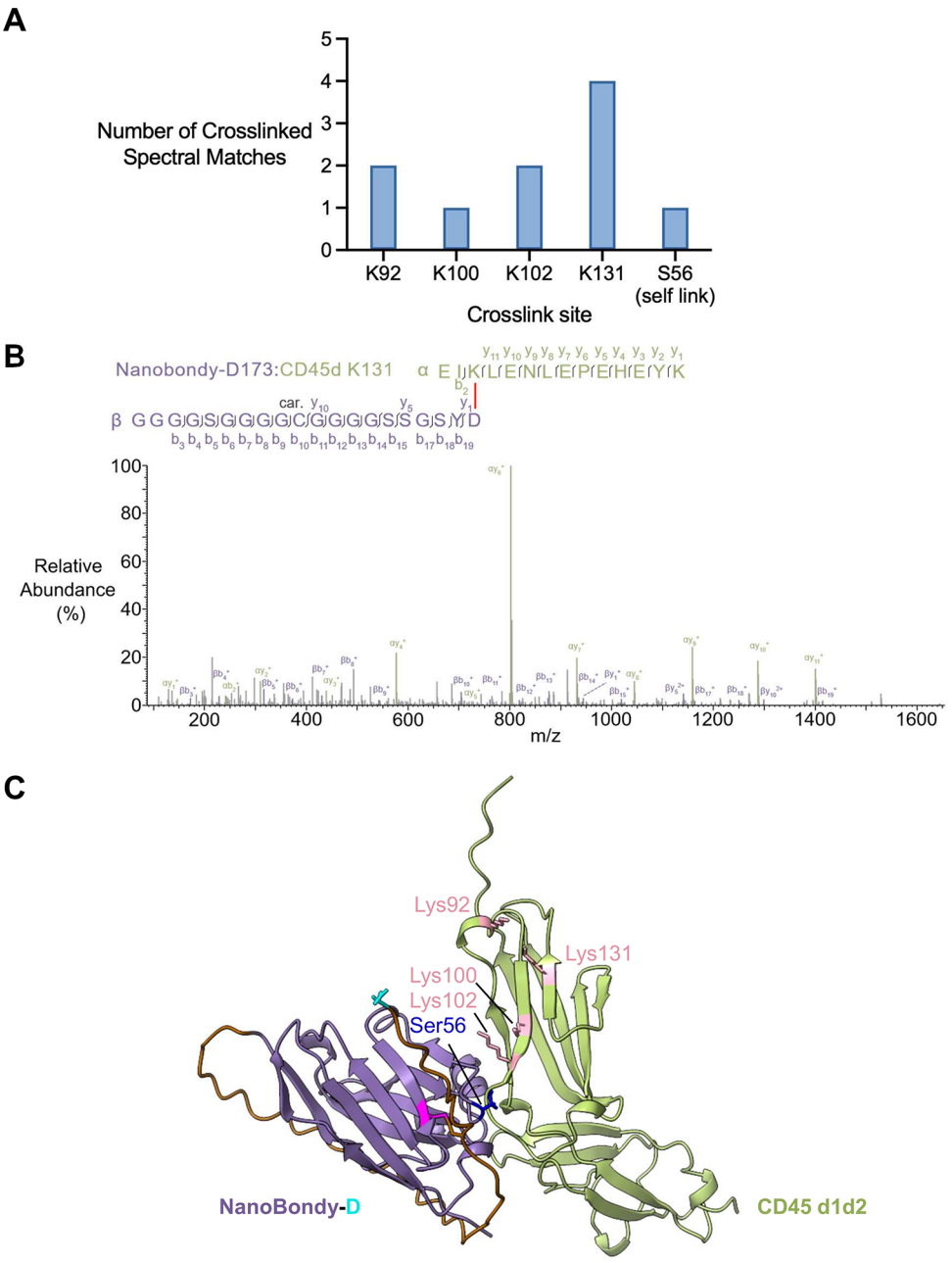

Figure 6. Mass spectrometry analysis of covalent conjugate between the NanoBondy and CD45d. (A) Dominant cross-linking sites. 2H5 R72C anti-CD45 NanoBondy was incubated with CD45d before cross-linking MS/MS. The number of identified cross-linked spectral matches for each NanoBondy cross-linking site on CD45 is shown. (B) Higher energy collision-induced dissociation (HCD) fragmentation spectrum of identified cross-link precursor ions corresponding to D173 (NanoBondy) to K131 (CD45d). Fragment ions matching fragmented cross-link (with cross-linker still intact) are annotated in bold, while peaks corresponding to fragments post-cross-link fragmentation are annotated with nonbold lines. "Car" indicates carbamidomethylation of cysteine. (C) Mapping of cross-link sites. AlphaFold prediction of NanoBondy (purple) bound to CD45d1d2 domains (green), highlighting cross-linking sites identified from the reactive aspartate (cyan) of the NanoBondy to target lysines (pink) or to serine (dark blue). Samples were run in technical triplicate. The cross-linking MS experiment was conducted twice.

reactive anti-CD45 NanoBondy (Figure 7C/D).[54] In addition to the standard (WT) DuoBondy, we also generated a DA variant, where the reactive aspartate residue of SPM is mutated to alanine. This DA variant is therefore capable of noncovalent binding but not calcium-mediated cleavage or conjugation. To test the DuoBondy reaction, human primary $CD8^+$ T cells were isolated from leukocyte blood cones. $CD8^+$ T cells were incubated with 1 μM DuoBondy or DuoBondy DA in the presence of calcium. We evaluated the reactivity of DuoBondy to the $CD8^+$ cell surface via Western blotting. The expected mass of the DuoBondy-D:CD45 conjugate is 217 kDa. When blotting for VHH, we consistently observed high molecular weight products following calcium addition that migrated from approximately 250 kDa to just below the 185 kDa marker, consistent with the reaction product between DuoBondy and CD45 (Figure 7C/D). We did not observe nonspecific bands, indicating that the DuoBondy reaction did not show promiscuous reactivity to other cell-surface proteins (Figure 7C). We observed conjugation only for the DuoBondy, with no covalent adduct detected for DuoBondy DA. These results

https://doi.org/10.1021/acs.bioconjchem.5c00519
Bioconjugate Chem. XXXX, XXX, XXX−XXX

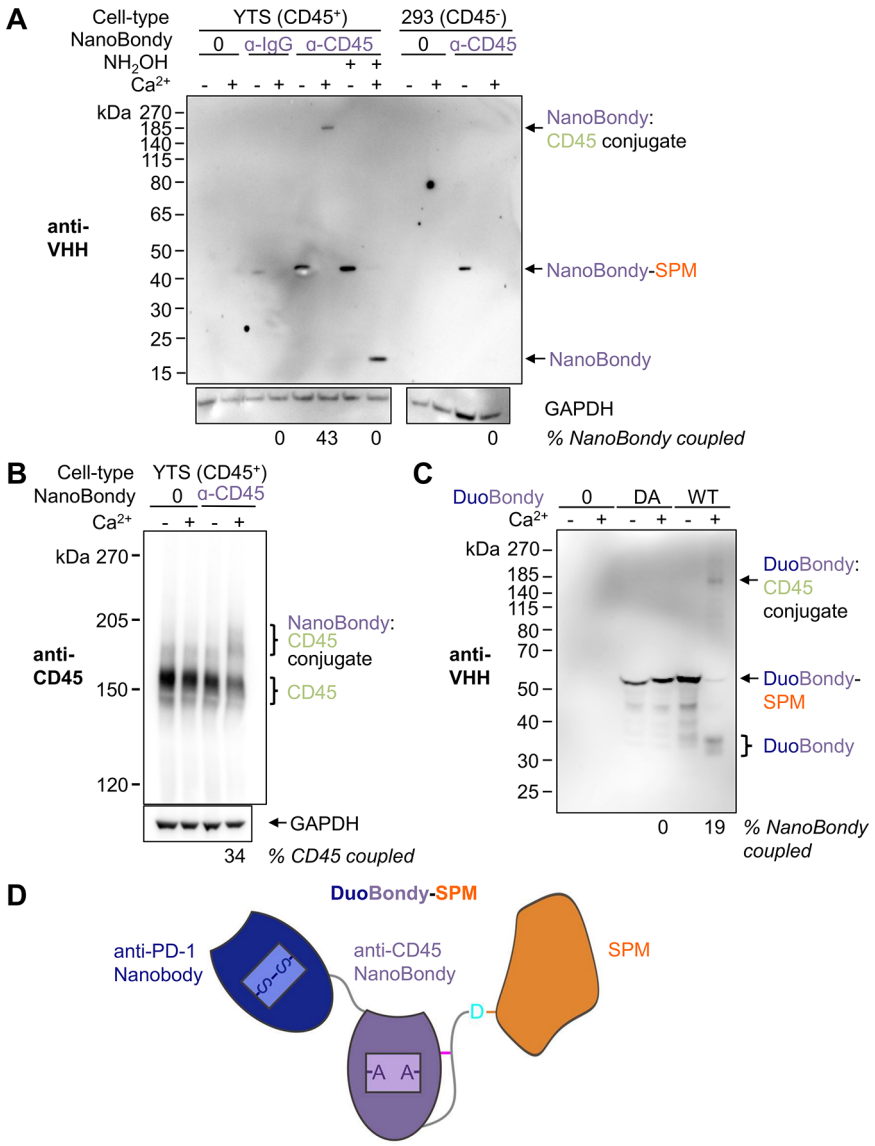

Figure 7. NanoBondy covalent conjugation at the cell surface. (A) Western blotting of NanoBondy reaction at the cell surface. Anti-CD45 NanoBondy at 5 μM was incubated with YTS cells or Expi293F cells for 1 h at 37 °C ± calcium. Covalent conjugation was evaluated by Western blot using an anti-VHH polyclonal antibody to detect the NanoBondy. Anti-IgG NanoBondy or hydroxylamine to react with the anhydride provided negative controls. Western blot to glyceraldehyde-3-phosphate dehydrogenase (GAPDH) was the loading control. The complete GAPDH blot is presented in Figure S6A. The experiment was conducted once. (B) YTS cells were stained as in (A), except with 25 μM anti-CD45 NanoBondy, and analyzed by Western blot using an anti-CD45 antibody. The CD45 band demonstrates an upward shift upon covalent conjugation with the a-CD45 NanoBondy. The full-length GAPDH blot is presented in Figure S6B. The experiment was conducted once. (C) Western blotting of the DuoBondy reaction on $CD8^+$ T cells. DuoBondy (WT) or DuoBondy (DA) at 1 μM was incubated with $CD8^+$ T cells for 40 min at 37 °C ± calcium. Covalent conjugation was evaluated by Western blot using an anti-VHH polyclonal antibody to detect the DuoBondy. Representative blot from two independent experiments. (D) DuoBondy consists of a nanobody binder (Nb102c3) to PD-1 (dark blue) fused N-terminally to the established covalently reacting anti-CD45 NanoBondy (purple) with SPM in orange.

demonstrate that NanoBondy technology allows covalent attachment of effector proteins to primary human cells and that fusion of an effector protein to the NanoBondy does not interfere with covalent cell conjugation.

■ DISCUSSION

Here, we have established NanoBondies, reengineering nanobodies for covalent reactivity through the inducible anhydride generation of NeissLock. We upgraded two different nanobodies to form covalent bonds with CD45. The reaction was compatible with different buffers and temperatures and showed specificity at the surface of an NK cell line and primary human $CD8^+$ T cells. Previous use of NeissLock depended on the existence of a high-resolution structure in the Protein Data Bank to guide the reaction.[40] Despite advances in computational structure prediction, there is still uncertainty in the prediction of protein binding interfaces, particularly for contacts through antibodies and nanobodies, where there are flexible loops and no evolutionary conservation.[55,56] This work demonstrates the harnessing of protein binders for covalent coupling, even where there is no experimental structure.

Binders can be upgraded to covalent reactivity by incorporating weak electrophiles into binding interfaces, either through direct chemical coupling[57] or unnatural amino acid

https://doi.org/10.1021/acs.bioconjchem.5c00519
Bioconjugate Chem. XXXX, XXX, XXX−XXX

mutagenesis.[33,58] Initial electrophiles, such as acrylamides, were highly effective for reacting with exposed cysteines at the protein−protein interface but inefficient with other side chains.[57] More recent use of SuFEx couples to a range of side chains, including lysine and tyrosine.[33,59] However, the lack of inducible reactivity may pose challenges for the sustained storage of such reagents. Similar chemical or genetic routes may also be taken to attach photo-cross-linkers onto binders, but ultraviolet light activation of reactivity is damaging to cell survival and effector function.[60,61] NeissLock reactivity is selectively induced under gentle conditions by adding extracellular levels of Ca^{2+}, and the components are fully genetically encoded, using only canonical amino acids, which promotes simple and scalable production. Efficient NeissLock-driven protein:protein conjugation has been demonstrated for various protein pairs. Factors such as target protein glycosylation or the availability of surface lysines for conjugation may impact the overall yield of NeissLock-mediated conjugation. We demonstrate that reducing the strength of the initial noncovalent interaction between the NanoBondy and CD45d through the introduction of point mutations in CD45d decreases the subsequent degree of conjugation, supporting the idea that the strength of the initial noncovalent protein/protein interaction is important for the efficiency of reaction.

Our quantitation of cross-link frequency to different sites on the target provides valuable insights into the reach and residue preference of the anhydride from the NanoBondy. Previous MS on anhydride reactivity from NeissLock only identified a dominant cross-link to a lysine,[40] but here we have quantified reactions to multiple lysine targets as well as a serine. This diverse range of possible sites for NeissLock coupling on the target is exciting, indicating that most proteins should be susceptible to ligation. Conversely, broad anhydride reactivity poses challenges in avoiding "own-goal" reaction sites on the NanoBondy itself when the highest reaction yield is desired. A limitation of NanoBondies is that competition between hydrolysis and coupling means this bioconjugation is unlikely to achieve near-quantitative target ligation, as may be achieved with SpyTag/SpyCatcher or HaloTag.[17,62]

Currently, our NanoBondy optimization pipeline involves testing a small set of different clamp locations, linker lengths, and own-goal lysine sites before validating the NanoBondy with the best expression, binding specificity, and reaction yield. Nanobodies or the related Sybodies are available for more than a thousand cellular targets,[63] so the NanoBondy strategy has the potential to be generalized in diverse biological contexts. Despite internal disulfide bonds in nanobodies, we achieved efficient clamping through a novel disulfide bond in Nano-Bondies. In many cases, the core disulfide in the nanobody was not necessary for folding and expression[64] and the clamp disulfide was well-formed in regular *E. coli* strains, not requiring strains optimized for an oxidizing cytosol.[65] Most binding scaffolds (e.g., antibodies, affibodies, and DARPins)[66] are like nanobodies in having the C-terminus away from the ligand-binding site, so it may be feasible in future work to use clamping to engineer these other platforms into NeissLock-based covalent binders.

CD45 represents an attractive initial target for covalent cell coupling because of its high expression on a wide range of hematopoietic cells and its stable surface expression.[14] Future work may explore anti-CD45 NanoBondies on other cell types, given the cancer-targeting potential of CAR-macrophages and CAR-neutrophils.[67] Future covalent targeting will also be valuable on red blood cells, which circulate for months and lack turnover of their plasma membrane.[35] Beyond cell therapy, in biomaterials,[68] biotransformation,[69] gene therapy,[70] and diagnostics,[71] target-specific irreversible coupling with NanoBondies may enable new opportunities for molecular tenacity.

■ ASSOCIATED CONTENT

Supporting Information

The Supporting Information is available free of charge at https://pubs.acs.org/doi/10.1021/acs.bioconjchem.5c00519.

Comprehensive methods and supplementary results, including amino acid sequence, MS, structure prediction, and fluorescence microscopy (PDF)

■ AUTHOR INFORMATION

Corresponding Author

Mark R. Howarth − *Department of Pharmacology, University of Cambridge, Cambridge CB2 1PD, U.K.; Engineering Biology Interdisciplinary Research Centre, University of Cambridge, Cambridge CB2 1GA, U.K.;* orcid.org/0000-0001-8870-7147; Email: mh2186@cam.ac.uk

Authors

Lasya R. Vankayala − *Department of Biochemistry, University of Oxford, Oxford OX1 3QU, U.K.; Department of Pharmacology, University of Cambridge, Cambridge CB2 1PD, U.K.; Engineering Biology Interdisciplinary Research Centre, University of Cambridge, Cambridge CB2 1GA, U.K.; Sir William Dunn School of Pathology, University of Oxford, Oxford OX1 3RE, U.K.*

Kish R. Adoni − *Institute of Structural and Molecular Biology, Division of Biosciences, University College London, London WC1E 6BT, U.K.; Institute of Structural and Molecular Biology, Birkbeck College, University of London, London WC1E 6BT, U.K.;* orcid.org/0000-0001-7390-501X

Sheryl Y. T. Lim − *Department of Biochemistry, University of Oxford, Oxford OX1 3QU, U.K.;* Present Address: Institute of Molecular and Cell Biology, Agency for Science, Technology and Research (A*STAR), 61 Biopolis Drive, Singapore 138673, Singapore; orcid.org/0000-0002-2606-9220

Tommy Dam − *Sir William Dunn School of Pathology, University of Oxford, Oxford OX1 3RE, U.K.*

Omer Dushek − *Sir William Dunn School of Pathology, University of Oxford, Oxford OX1 3RE, U.K.*

Konstantinos Thalassinos − *Institute of Structural and Molecular Biology, Division of Biosciences, University College London, London WC1E 6BT, U.K.; Institute of Structural and Molecular Biology, Birkbeck College, University of London, London WC1E 6BT, U.K.;* orcid.org/0000-0001-5072-8428

Complete contact information is available at: https://pubs.acs.org/10.1021/acs.bioconjchem.5c00519

Author Contributions

L.R.V. performed all experiments, except K.R.A. who performed cross-linking MS, and T.D., who performed confocal microscopy. S.Y.T.L. developed the FrpA fusion. L.R.V., O.D., K.R.A., K.T., and M.R.H. designed the project.

https://doi.org/10.1021/acs.bioconjchem.5c00519
Bioconjugate Chem. XXXX, XXX, XXX−XXX

L.R.V. and M.R.H. wrote the manuscript. All authors read and approved the manuscript.

Notes

The authors declare the following competing financial interest(s): S.Y.T.L. and M.R.H. are inventors on patent applications regarding inducible anhydride formation for targeted ligation (UK Intellectual Property Office Patent Application No. 2504781.2 and 2003683.6). All other authors do not have competing interests.

■ ACKNOWLEDGMENTS

L.R.V. was funded by MSD. M.R.H. was funded by the Engineering and Physical Sciences Research Council (EPSRC EP/W01565X/1). K.A. is funded by a Wellcome Collaborative Award in Science (209250/Z/17/Z) to K.T. The mass spectrometer used for cross-linking was funded by a Wellcome Trust Multiuser Equipment grant (221521/Z/20/Z) to K.T. S.Y.T.L. was funded by an A*STAR studentship. This work was supported by the Wellcome Trust (207537/Z/17/Z, 301534/Z/23/Z). We thank Dr. Anthony Tumber (University of Oxford, Department of Chemistry) for assistance with intact protein mass spectrometry, supported by the Biotechnology and Biological Sciences Research Council (BBSRC BB/R000344/1). We thank the flow cytometry facility staff at the University of Cambridge School of the Biological Sciences for the technical expertise provided. AlphaFold2-multimer docking was performed using resources provided by the Cambridge Service for Data Driven Discovery (CSD3). CSD3 is operated by the University of Cambridge Research Computing Service, provided by Dell EMC and Intel, using Tier-2 funding from the EPSRC (capital grant EP/T022159/1) and DiRAC funding from the Science and Technology Facilities Council. We would like to thank Dr. Alan Wainman and the Dunn School Bioimaging Facility.

■ REFERENCES

(1) Keeble, A. H.; Howarth, M. Power to the Protein: Enhancing and Combining Activities Using the Spy Toolbox. *Chem. Sci.* **2020**, *11* (28), 7281−7291.

(2) Oostindie, S. C.; Lazar, G. A.; Schuurman, J.; Parren, P. W. H. I. Avidity in Antibody Effector Functions and Biotherapeutic Drug Design. *Nat. Rev. Drug Discovery* **2022**, *21* (10), 715−735.

(3) Khan, S. H.; Choi, Y.; Veena, M.; Lee, J. K.; Shin, D. S. Advances in CAR T Cell Therapy: Antigen Selection, Modifications, and Current Trials for Solid Tumors. *Front. Immunol.* **2025**, *15*, 1489827.

(4) Brenner, J. S.; Mitragotri, S.; Muzykantov, V. R. Red Blood Cell Hitchhiking: A Novel Approach for Vascular Delivery of Nanocarriers. *Annu. Rev. Biomed. Eng.* **2021**, *23* (1), 225−248.

(5) Albelda, S. M. CAR T Cell Therapy for Patients with Solid Tumours: Key Lessons to Learn and Unlearn. *Nat. Rev. Clin Oncol.* **2024**, *21* (1), 47−66.

(6) D'Aloia, M. M.; Zizzari, I. G.; Sacchetti, B.; Pierelli, L.; Alimandi, M. CAR-T Cells: The Long and Winding Road to Solid Tumors. *Cell Death Dis.* **2018**, *9* (3), 282.

(7) Guzman, G.; Reed, M. R.; Bielamowicz, K.; Koss, B.; Rodriguez, A. CAR-T Therapies in Solid Tumors: Opportunities and Challenges. *Curr. Oncol. Rep.* **2023**, *25* (5), 479−489.

(8) Hurton, L. V.; Singh, H.; Najjar, A. M.; Switzer, K. C.; Mi, T.; Maiti, S.; Olivares, S.; Rabinovich, B.; Huls, H.; Forget, M.-A.; et al. Tethered IL-15 Augments Antitumor Activity and Promotes a Stem-Cell Memory Subset in Tumor-Specific T Cells. *Proc. Natl. Acad. Sci. U.S.A.* **2016**, *113* (48), No. E7788−E7797.

(9) Jones, D. S.; Nardozzi, J. D.; Sackton, K. L.; Ahmad, G.; Christensen, E.; Ringgaard, L.; Chang, D.-K.; Jaehger, D. E.; Konakondla, J. V.; Wiinberg, M.; Stokes, K. L.; Pratama, A.; Sauer, K.; Andresen, T. L. Cell Surface−Tethered IL-12 Repolarizes the Tumor Immune Microenvironment to Enhance the Efficacy of Adoptive T Cell Therapy. *Sci. Adv.* **2022**, *8* (17), No. eabi8075.

(10) Zhao, Y.; Dong, Y.; Yang, S.; Tu, Y.; Wang, C.; Li, J.; Yuan, Y.; Lian, Z. Bioorthogonal Equipping CAR-T Cells with Hyaluronidase and Checkpoint Blocking Antibody for Enhanced Solid Tumor Immunotherapy. *ACS Cent. Sci.* **2022**, *8* (5), 603−614.

(11) Stephan, M.; Stephan, S.; Bak, P.; Chen, J.; Irvine, D. J. Synapse-Directed Delivery of Immunomodulators Using T-Cell-Conjugated Nanoparticles. *Biomaterials* **2012**, *33* (23), 5776−5787.

(12) Luo, Y.; Chen, Z.; Sun, M.; Li, B.; Pan, F.; Ma, A.; Liao, J.; Yin, T.; Tang, X.; Huang, G.; Zhang, B.; Pan, H.; Zheng, M.; Cai, L. IL-12 Nanochaperone-Engineered CAR T Cell for Robust Tumor-Immunotherapy. *Biomaterials* **2022**, *281*, 121341.

(13) Liu, Y.; Adu-Berchie, K.; Brockman, J. M.; Pezone, M.; Zhang, D. K. Y.; Zhou, J.; Pyrdol, J. W.; Wang, H.; Wucherpfennig, K. W.; Mooney, D. J. Cytokine Conjugation to Enhance T Cell Therapy. *Proc. Natl. Acad. Sci. U.S.A.* **2023**, *120* (1), No. e2213222120.

(14) Zheng, Y.; Tang, L.; Mabardi, L.; Kumari, S.; Irvine, D. J. Enhancing Adoptive Cell Therapy of Cancer through Targeted Delivery of Small-Molecule Immunomodulators to Internalizing or Noninternalizing Receptors. *ACS Nano* **2017**, *11* (3), 3089−3100.

(15) Stephan, M.; Moon, J.; Um, S. H.; Bershteyn, A.; Irvine, D. Therapeutic Cell Engineering with Surface-Conjugated Synthetic Nanoparticles. *Nat. Med.* **2010**, *16* (9), 1035−1041.

(16) Tang, L.; Zheng, Y.; Melo, M. B.; Mabardi, L.; Castaño, A. P.; Xie, Y.-Q.; Li, N.; Kudchodkar, S. B.; Wong, H. C.; Jeng, E. K.; Maus, M. V.; Irvine, D. J. Enhancing T Cell Therapy through TCR-Signaling-Responsive Nanoparticle Drug Delivery. *Nat. Biotechnol.* **2018**, *36* (8), 707−716.

(17) Los, G. V.; Encell, L. P.; McDougall, M. G.; Hartzell, D. D.; Karassina, N.; Zimprich, C.; Wood, M. G.; Learish, R.; Ohana, R. F.; Urh, M.; Simpson, D.; Mendez, J.; Zimmerman, K.; Otto, P.; Vidugiris, G.; Zhu, J.; Darzins, A.; Klaubert, D. H.; Bulleit, R. F.; Wood, K. V. HaloTag: A Novel Protein Labeling Technology for Cell Imaging and Protein Analysis. *ACS Chem. Biol.* **2008**, *3* (6), 373−382.

(18) Keppler, A.; Gendreizig, S.; Gronemeyer, T.; Pick, H.; Vogel, H.; Johnsson, K. A General Method for the Covalent Labeling of Fusion Proteins with Small Molecules in Vivo. *Nat. Biotechnol.* **2003**, *21* (1), 86−89.

(19) Sun, F.; Zhang, W.-B. Genetically Encoded Click Chemistry. *Chin. J. Chem.* **2020**, *38* (8), 894−896.

(20) Humberg, C.; Yilmaz, Z.; Fitzian, K.; Dörner, W.; Kümmel, D.; Mootz, H. D. A Cysteine-Less and Ultra-Fast Split Intein Rationally Engineered from Being Aggregation-Prone to Highly Efficient in Protein Trans-Splicing. *Nat. Commun.* **2025**, *16* (1), 2723.

(21) Mao, H.; Hart, S. A.; Schink, A.; Pollok, B. A. Sortase-Mediated Protein Ligation: A New Method for Protein Engineering. *J. Am. Chem. Soc.* **2004**, *126* (9), 2670−2671.

(22) Liu, X.; Wen, J.; Yi, H.; Hou, X.; Yin, Y.; Ye, G.; Wu, X.; Jiang, X. Split Chimeric Antigen Receptor-Modified T Cells Targeting Glypican-3 Suppress Hepatocellular Carcinoma Growth with Reduced Cytokine Release. *Ther. Adv. Med. Oncol.* **2020**, *12*, 175883592091034.

(23) Sutherland, A. R.; Owens, M. N.; Geyer, C. R. Modular Chimeric Antigen Receptor Systems for Universal CAR T Cell Retargeting. *Int. J. Mol. Sci.* **2020**, *21* (19), 7222.

(24) Minutolo, N. G.; Sharma, P.; Poussin, M.; Shaw, L. C.; Brown, D. P.; Hollander, E. E.; Smole, A.; Rodriguez-Garcia, A.; Hui, J. Z.; Zappala, F.; Tsourkas, A.; Powell, D. J. Quantitative Control of Gene-Engineered T-Cell Activity through the Covalent Attachment of Targeting Ligands to a Universal Immune Receptor. *J. Am. Chem. Soc.* **2020**, *142* (14), 6554−6568.

(25) Rahikainen, R.; Rijal, P.; Tan, T. K.; Wu, H.; Andersson, A. C.; Barrett, J. R.; Bowden, T. A.; Draper, S. J.; Townsend, A. R.; Howarth, M. Overcoming Symmetry Mismatch in Vaccine Nanoassembly through Spontaneous Amidation. *Angew. Chem. Int. Ed.* **2021**, *60* (1), 321−330.

(26) Bishani, A.; Chernolovskaya, E. L. Activation of Innate Immunity by Therapeutic Nucleic Acids. *Int. J. Mol. Sci.* **2021**, *22* (24), 13360.
(27) Bonifant, C. L.; Jackson, H. J.; Brentjens, R. J.; Curran, K. J. Toxicity and Management in CAR T-Cell Therapy. *Mol. Ther. Oncolytics* **2016**, *3*, 16011.
(28) Hamdy, N.; Goustin, A. S.; Desaulniers, J.-P.; Li, M.; Chow, C. S.; Al-Katib, A. Sheep Red Blood Cells Armed with Anti-CD20 Single-Chain Variable Fragments (scFvs) Fused to a Glycosylphosphatidylinositol (GPI) Anchor: A Strategy to Target CD20-Positive Tumor Cells. *J. Immunol. Methods* **2005**, *297* (1−2), 109−124.
(29) White, S.; Vonheijne, G. Transmembrane Helices before, during, and after Insertion. *Curr. Opin. Struct. Biol.* **2005**, *15* (4), 378−386.
(30) Reinisch, K. M.; Prinz, W. A. Mechanisms of Nonvesicular Lipid Transport. *J. Cell Biol.* **2021**, *220* (3), No. e202012058.
(31) Yu, B.; Li, S.; Tabata, T.; Wang, N.; Cao, L.; Kumar, G. R.; Sun, W.; Liu, J.; Ott, M.; Wang, L. Accelerating PERx Reaction Enables Covalent Nanobodies for Potent Neutralization of SARS-CoV-2 and Variants. *Chem* **2022**, *8* (10), 2766−2783.
(32) Yu, B.; Cao, L.; Li, S.; Klauser, P. C.; Wang, L. The Proximity-Enabled Sulfur Fluoride Exchange Reaction in the Protein Context. *Chem. Sci.* **2023**, *14* (29), 7913−7921.
(33) Li, Q.; Chen, Q.; Klauser, P. C.; Li, M.; Zheng, F.; Wang, N.; Li, X.; Zhang, Q.; Fu, X.; Wang, Q.; et al. Developing Covalent Protein Drugs via Proximity-Enabled Reactive Therapeutics. *Cell* **2020**, *182* (1), P85−97.E16.
(34) De Bank, P. A.; Kellam, B.; Kendall, D. A.; Shakesheff, K. M. Surface Engineering of Living Myoblasts via Selective Periodate Oxidation. *Biotechnol. Bioeng.* **2003**, *81* (7), 800−808.
(35) Glassman, P. M.; Hood, E. D.; Ferguson, L. T.; Zhao, Z.; Siegel, D. L.; Mitragotri, S.; Brenner, J. S.; Muzykantov, V. R. Red Blood Cells: The Metamorphosis of a Neglected Carrier into the Natural Mothership for Artificial Nanocarriers. *Adv. Drug Delivery Rev.* **2021**, *178*, 113992.
(36) Bao, G.; Tang, M.; Zhao, J.; Zhu, X. Nanobody: A Promising Toolkit for Molecular Imaging and Disease Therapy. *EJNMMI Res.* **2021**, *11* (1), 6.
(37) Asaadi, Y.; Jouneghani, F. F.; Janani, S.; Rahbarizadeh, F. A Comprehensive Comparison between Camelid Nanobodies and Single Chain Variable Fragments. *Biomark. Res.* **2021**, *9* (1), 87.
(38) Tack, L.; Miret-Casals, L.; Zwaenepoel, O.; Cadoni, E.; Van Troys, M.; Gettemans, J.; Madder, A. Development of "Furan Warhead"-Equipped Antagonistic Nanobodies for Covalent Cross-Linking to the Epidermal Growth Factor Receptor. *Bioconjugate Chem.* **2025**, *36* (8), 1649−1660.
(39) Gao, W.; Cho, E.; Liu, Y.; Lu, Y. Advances and Challenges in Cell-Free Incorporation of Unnatural Amino Acids Into Proteins. *Front. Pharmacol.* **2019**, *10*, 611.
(40) Scheu, A.; Lim, S. Y. T.; Metzner, F. J.; Mohammed, S.; Howarth, M. NeissLock Provides an Inducible Protein Anhydride for Covalent Targeting of Endogenous Proteins. *Nat. Commun.* **2021**, *12* (1), 717.
(41) Lim, S.; Keeble, A. H.; Howarth, M. R. Split NeissLock with Spy-Acceleration Arms Mammalian Proteins for Anhydride-Mediated Cell Ligation. *ACS Chem. Biol.* **2025**, *20*, 2475.
(42) Sviridova, E.; Rezacova, P.; Bondar, A.; Veverka, V.; Novak, P.; Schenk, G.; Svergun, D. I.; Kuta Smatanova, I.; Bumba, L. Structural Basis of the Interaction between the Putative Adhesion-Involved and Iron-Regulated FrpD and FrpC Proteins of Neisseria Meningitidis. *Sci. Rep.* **2017**, *7* (1), 40408.
(43) Borowska, M. T.; Liu, L. D.; Caveney, N. A.; Jude, K. M.; Kim, W.-J.; Masubuchi, T.; Hui, E.; Majzner, R. G.; Garcia, K. C. Orientation-Dependent CD45 Inhibition with Viral and Engineered Ligands. *Sci. Immunol.* **2024**, *9* (100), No. eadp0707.
(44) Rokkam, D.; Lupardus, P. J. Discovery and Characterization of Llama VHH Targeting the RO Form of Human CD45. *bioRxiv*. 2020.
(45) Keeble, A. H.; Turkki, P.; Stokes, S.; Khairil Anuar, I. N. A.; Rahikainen, R.; Hytönen, V. P.; Howarth, M. Approaching Infinite Affinity through Engineering of Peptide−Protein Interaction. *Proc. Natl. Acad. Sci. U.S.A.* **2019**, *116* (52), 26523−26533.
(46) Vester, S. K.; Rahikainen, R.; Khairil Anuar, I. N. A.; Hills, R. A.; Tan, T. K.; Howarth, M. SpySwitch Enables pH- or Heat-Responsive Capture and Release for Plug-and-Display Nanoassembly. *Nat. Commun.* **2022**, *13* (1), 3714.
(47) Bryant, P.; Pozzati, G.; Elofsson, A. Improved Prediction of Protein-Protein Interactions Using AlphaFold2. *Nat. Commun.* **2022**, *13* (1), 1265.
(48) Evans, R.; O'Neill, M.; Pritzel, A.; Antropova, N.; Senior, A.; Green, T.; Žídek, A.; Bates, R.; Blackwell, S.; Yim, J.et al. Protein Complex Prediction With AlphaFold-Multimer. *bioRxiv*. 2022.
(49) Zhong, B.; Su, X.; Wen, M.; Zuo, S.; Hong, L.; Lin, J. ParaFold: Paralleling AlphaFold For Large-Scale Predictions. *arXiv*. 2021.
(50) Breitwieser, G. E. Extracellular Calcium as an Integrator of Tissue Function. *Int. J. Biochem. Cell Biol.* **2008**, *40* (8), 1467−1480.
(51) Hermiston, M. L.; Xu, Z.; Weiss, A. CD45: A Critical Regulator of Signaling Thresholds in Immune Cells. *Annu. Rev. Immunol.* **2003**, *21* (1), 107−137.
(52) Savchenko, A. A.; Tikhonova, E.; Kudryavtsev, I.; Kudlay, D.; Korsunsky, I.; Beleniuk, V.; Borisov, A. TREC/KREC Levels and T and B Lymphocyte Subpopulations in COVID-19 Patients at Different Stages of the Disease. *Viruses* **2022**, *14* (3), 646.
(53) Kalinin, R. S.; Ukrainskaya, V. M.; Chumakov, S. P.; Moysenovich, A. M.; Tereshchuk, V. M.; Volkov, D. V.; Pershin, D. S.; Maksimov, E. G.; Zhang, H.; Maschan, M. A.; Rubtsov, Y. P.; Stepanov, A. V. Engineered Removal of PD-1 From the Surface of CD19 CAR-T Cells Results in Increased Activation and Diminished Survival. *Front. Mol. Biosci.* **2021**, *8*, 745286.
(54) Fernandes, R. A.; Su, L.; Nishiga, Y.; Ren, J.; Bhuiyan, A. M.; Cheng, N.; Kuo, C. J.; Picton, L. K.; Ohtsuki, S.; Majzner, R. G.; Rietberg, S. P.; Mackall, C. L.; Yin, Q.; Ali, L. R.; Yang, X.; Savvides, C. S.; Sage, J.; Dougan, M.; Garcia, K. C. Immune Receptor Inhibition through Enforced Phosphatase Recruitment. *Nature* **2020**, *586* (7831), 779−784.
(55) Fernández-Quintero, M. L.; Kokot, J.; Waibl, F.; Fischer, A.-L. M.; Quoika, P. K.; Deane, C. M.; Liedl, K. R. Challenges in Antibody Structure Prediction. *mAbs* **2023**, *15* (1), 2175319.
(56) Erasmus, M. F.; Spector, L.; Ferrara, F.; DiNiro, R.; Pohl, T. J.; Perea-Schmittle, K.; Wang, W.; Tessier, P. M.; Richardson, C.; Turner, L.; Kumar, S.; Bedinger, D.; Sormanni, P.; Fernández-Quintero, M. L.; Ward, A. B.; Loeffler, J. R.; Swanson, O. M.; Deane, C. M.; Raybould, M. I. J.; Evers, A.; Sellmann, C.; Bachas, S.; Ruffolo, J.; Nastri, H. G.; Ramesh, K.; Sørensen, J.; Croasdale-Wood, R.; Hijano, O.; Leal-Lopes, C.; Shahsavarian, M.; Qiu, Y.; Marcatili, P.; Vernet, E.; Akbar, R.; Friedensohn, S.; Wagner, R.; Kurella, V. B.; Malhotra, S.; Kumar, S.; Kidger, P.; Almagro, J. C.; Furfine, E.; Stanton, M.; Graff, C. P.; Villalba, S. D.; Tomszak, F.; Teixeira, A. A. R.; Hopkins, E.; Dovner, M.; D'Angelo, S.; Bradbury, A. R. M. AIntibody: An Experimentally Validated in Silico Antibody Discovery Design Challenge. *Nat. Biotechnol.* **2024**, *42* (11), 1637−1642.
(57) Holm, L.; Moody, P.; Howarth, M. Electrophilic Affibodies Forming Covalent Bonds to Protein Targets. *J. Biol. Chem.* **2009**, *284* (47), 32906−32913.
(58) De La Torre, D.; Chin, J. W. Reprogramming the Genetic Code. *Nat. Rev. Genet.* **2021**, *22* (3), 169−184.
(59) Zhang, H.; Han, Y.; Yang, Y.; Lin, F.; Li, K.; Kong, L.; Liu, H.; Dang, Y.; Lin, J.; Chen, P. R. Covalently Engineered Nanobody Chimeras for Targeted Membrane Protein Degradation. *J. Am. Chem. Soc.* **2021**, *143* (40), 16377−16382.
(60) Tyrrell, R. M. Induction of Pyrimidine Dimers In Bacterial DNA by 365 nm Radiation. *Photochem. Photobiol.* **1973**, *17* (1), 69−73.
(61) Andley, U. P.; Lewis, R. M.; Reddan, J. R.; Kochevar, I. E. Action Spectrum for Cytotoxicity in the UVA- and UVB-Wavelength Region in Cultured Lens Epithelial Cells. *Invest. Ophthalmol. Vis. Sci.* **1994**, *35* (2), 367−373 https://iovs.arvojournals.org/article.aspx?articleid=2161027.

https://doi.org/10.1021/acs.bioconjchem.5c00519
Bioconjugate Chem. XXXX, XXX, XXX−XXX

(62) Veggiani, G.; Nakamura, T.; Brenner, M. D.; Gayet, R. V.; Yan, J.; Robinson, C. V.; Howarth, M. Programmable Polyproteams Built Using Twin Peptide Superglues. *Proc. Natl. Acad. Sci. U.S.A.* **2016**, *113* (5), 1202−1207.
(63) Zimmermann, I.; Egloff, P.; Hutter, C. A. J.; Kuhn, B. T.; Bräuer, P.; Newstead, S.; Dawson, R. J. P.; Geertsma, E. R.; Seeger, M. A. Generation of Synthetic Nanobodies against Delicate Proteins. *Nat. Protoc.* **2020**, *15* (5), 1707−1741.
(64) Kunz, P.; Zinner, K.; Mücke, N.; Bartoschik, T.; Muyldermans, S.; Hoheisel, J. D. The Structural Basis of Nanobody Unfolding Reversibility and Thermoresistance. *Sci. Rep.* **2018**, *8* (1), 7934.
(65) Berkmen, M. Production of Disulfide-Bonded Proteins in Escherichia Coli. *Protein Expression Purif.* **2012**, *82* (1), 240−251.
(66) Gebauer, M.; Skerra, A. Engineered Protein Scaffolds as Next-Generation Therapeutics. *Annu. Rev. Pharmacol. Toxicol.* **2020**, *60* (1), 391−415.
(67) Liang, Y.; Xu, Q.; Gao, Q. Advancing CAR-Based Immunotherapies in Solid Tumors: CAR- Macrophages and Neutrophils. *Front. Immunol.* **2023**, *14*, 1291619.
(68) Wang, X.-W.; Zhang, W.-B. Chemical Topology and Complexity of Protein Architectures. *Trends Biochem. Sci.* **2018**, *43* (10), 806−817.
(69) Pedram, K.; Shon, D. J.; Tender, G. S.; Mantuano, N. R.; Northey, J. J.; Metcalf, K. J.; Wisnovsky, S. P.; Riley, N. M.; Forcina, G. C.; Malaker, S. A.; Kuo, A.; George, B. M.; Miller, C. L.; Casey, K. M.; Vilches-Moure, J. G.; Ferracane, M. J.; Weaver, V. M.; Läubli, H.; Bertozzi, C. R. Design of a Mucin-Selective Protease for Targeted Degradation of Cancer-Associated Mucins. *Nat. Biotechnol.* **2024**, *42* (4), 597−607.
(70) Eichhoff, A. M.; Börner, K.; Albrecht, B.; Schäfer, W.; Baum, N.; Haag, F.; Körbelin, J.; Trepel, M.; Braren, I.; Grimm, D.; et al. Nanobody-Enhanced Targeting of AAV Gene Therapy Vectors. *Mol. Ther.−Methods Clin. Dev.* **2019**, *15*, P211−220.
(71) Bocancia-Mateescu, L.-A.; Stan, D.; Mirica, A.-C.; Ghita, M. G.; Stan, D.; Ruta, L. L. Nanobodies as Diagnostic and Therapeutic Tools for Cardiovascular Diseases (CVDs). *Pharmaceuticals* **2023**, *16* (6), 863.

https://doi.org/10.1021/acs.bioconjchem.5c00519
Bioconjugate Chem. XXXX, XXX, XXX−XXX

Supplementary Methods

NanoBondy Reaction through NeissLock Anhydride Allows Covalent Immune Cell Decoration

Lasya R. Vankayala[1,2,3,4], Kish R. Adoni[5,6], Sheryl Y.T. Lim[1,7], Tommy Dam[4], Omer Dushek[4], Konstantinos Thalassinos[5,6], and Mark R. Howarth[2,3]*

[1]Department of Biochemistry, University of Oxford, South Parks Road, Oxford, OX1 3QU, UK.
[2]Department of Pharmacology, University of Cambridge, Tennis Court Road, Cambridge, CB2 1PD, UK.
[3]Engineering Biology Interdisciplinary Research Centre, University of Cambridge, Cambridge, CB2 1GA, UK.
[4]Sir William Dunn School of Pathology, University of Oxford, South Parks Road, Oxford, OX1 3RE, UK.
[5]Institute of Structural and Molecular Biology, Division of Biosciences, University College London, London, WC1E 6BT, UK.
[6]Institute of Structural and Molecular Biology, Birkbeck College, University of London, London, WC1E 6BT, UK.
[7]Current address: Institute of Molecular and Cell Biology, Agency for Science, Technology and Research (A*STAR), 61 Biopolis Drive, Singapore 138673, Singapore.

*Corresponding author:
Mark Howarth,
Department of Pharmacology,
University of Cambridge,
Tennis Court Road,
Cambridge,
CB2 1PD,
UK
E-mail: mh2186@cam.ac.uk

Plasmids and cloning
PCR was conducted using Q5 High-Fidelity 2× Master Mix (New England Biolabs). DNA primers and gBlock gene fragments were ordered from Integrated DNA Technologies. All open reading frames were verified by Sanger sequencing (Source Bioscience and Azenta). The CD45 nanobody sequences were as described[72]. 1E4, 2H5, 2F8, 1G4 and 1G1 gBlock gene fragments were cloned into pET28a containing a C-terminal SpyTag003 (RGVPHIVMVDAYKRYK)[73] using Gibson assembly, yielding pET28a-1E4-SpyTag003 (GenBank accession no. PX392308), pET28a 2H5-SpyTag003 (GenBank accession no. PX392309), pET28a-2F8-SpyTag003 (GenBank accession no. PX392310), pET28a-1G1-SpyTag003 (GenBank accession no. PX392311) and pET28a-1G4-SpyTag003 (GenBank accession no. PX392312). pET28a-NanoBondy 2H5(R72C) (GenBank accession no. PX392314, Addgene plasmid ID 247051) contains the anti-CD45 nanobody 2H5 with mutations C22A, C96A, R72C, K76R, followed by a flexible linker containing SpyTag003 (9 residues between the cysteine clamp and the reactive aspartate), then the sequence for full-length FrpA SPM and a C-tag[74]. Variants were made based on pET28a-NanoBondy 2H5(R72C) with altered clamp sites: K76C (GenBank accession no. PX392313) and G118C

(GenBank accession no. PX392315). The anti-CD45 2H5 R72C NanoBondy-His_6 variant was made based on pET28a-NanoBondy 2H5(R72C) with a His_6-tag in place of the C-tag. FrpA SPM consists of amino acids 298-543 of FrpA from *Neisseria meningitidis* serotype C (UniProt: P55126). 2F8 NanoBondy (C22A, C96A, N74C) (GenBank accession no. PX392316) was generated by Gibson assembly from pET28a-2F8(C22A, C96A)-SpyTag003. For generation of the anti-mouse IgG NanoBondy, the nanobody TP1170[75] with C22A and C96A mutations was ordered as a gBlock and cloned into pET28a-NanoBondy 2H5(R72C) with TP1170(C22A, C96A) replacing 2H5(C22A, C96A, R72C). pET28a TP1170 K98C IgG NanoBondy variant (GenBank accession no. PX392317) was used for subsequent experimentation.

pET28a-NanoBondy 2H5(R72C) was used as the parental construct for all 2H5 NanoBondy linker variants. Linker variants were named according to the number of residues between the cysteine clamp and the reactive aspartate. To clone linker variants of the 2H5 NanoBondy, the linker following SpyTag003 (GGGGSGGGGCGGGGSSGSY, 9 residue) was modified via Gibson Assembly to yield the following: GGGGSGGGGCGSY (3 residue), GGGGSGGGGCGSSGSY (6 residue), GGGGSGGGGCGGGGSSGASGSY (12 residue), and GGGGSGGGGCGGGGSSGASGAGSGSGSY (18 residue).

For the anti-PD-1 DuoBondy, a gBlock gene fragment of the anti-PD-1 nanobody Nb102c3[76] was ordered from Integrated DNA Technologies, then inserted N-terminal to the NanoBondy sequence using Gibson assembly. Nb102c3 and the NanoBondy sequence were separated by a GGGGSSGSYGSY linker. The DuoBondy expression vector is pET28a containing a C-terminal His_6. We further modified the DuoBondy sequence by replacing the loop-internal SpyTag003 with a GS linker of equivalent length. We then generated anti-PD-1 DuoBondy (DA) by mutating the reactive aspartate of the FrpA sequence to an alanine. Nanobodies, NanoBondies and DuoBondies were cloned in competent *E. coli* DH5α cells. pLEXm-hCD45d1d2 was a kind gift from Simon Davis, University of Oxford[77]. pLEXm-hCD45d1d2-AviTag was cloned by inserting the sequence for AviTag C-terminally to the coding sequence for domains 1 and 2 of human CD45, using restriction enzyme cloning. Complementary oligonucleotides encoding the AviTag sequence were annealed at equimolar concentration, then phosphorylated by T4 polynucleotide kinase (New England Biolabs). The hCD45d1d2 vector was also digested using KpnI and XhoI and was simultaneously incubated with Shrimp Alkaline Phosphatase (rSAP). Enzymes were heat-killed at 80 ºC for 20 min and digestion products were purified using a Monarch PCR and DNA cleanup kit (New England Biolabs). Insert and vector fragments were ligated using T4 DNA ligase (New England Biolabs) for 16 h at 18 ºC. pLEXm-hCD45d (GenBank accession no. PX392318, Addgene plasmid ID 247052), pLEXm-hCD45d(I104R) and pLEXm-hCD45d(E105R) were cloned by inserting the sequence for MBP C-terminal to the hCD45d1d2 (WT), hCD45d1d2(I104R) or hCD45d1d2(E105R) sequence via restriction enzyme cloning. The MBP gene was amplified via PCR, using primers to insert *KpnI* and *XhoI* sites. The MBP PCR product was purified using a Monarch PCR and DNA cleanup kit (New England Biolabs), then digested using KpnI and XhoI (New England Biolabs). The pLEXm-hCD45d1d2 vector was also digested using KpnI and XhoI and was simultaneously incubated with rSAP. Enzymes were heat-killed at 80 ºC for 20 min. Insert and vector fragments were ligated using T4 DNA ligase (New England Biolabs) for 16 h at 18 ºC. CD45d was cloned in New England Biolab Turbo cells.

For mouse CD45d1d2 (mCD45d1d2), a gBlock gene fragment of residues 203-375 of the mouse CD45 sequence was ordered from Integrated DNA Technologies. The mCD45d1d2 gene fragment was inserted by Gibson Assembly into a pcDNA3.1 vector downstream of a tPA signal sequence with a C-terminal His_6 tag for purification and AviTag for site-specific biotinylation. mCD45d1d2 was cloned in New England Biolab Turbo cells.

pET28a-His6-ODC-Ctag was previously described[78] and consists of human ODC1 (UniProt P11926) with an N-terminal His_6 tag and a C-terminal C-tag, cloned in pET28a (GenBank MW364944, Addgene plasmid ID 163614). pET28a-SpyTag003-sfGFP was also previously described[73] (Addgene plasmid ID 133454). SpyCatcher002-MBP was previously described[79] (GenBank MF974389 and Addgene plasmid ID 102831) and consists of SpyCatcher002 fused N-terminally to MBP in pET28. pET28a-nanoHER2-SpyTag003-His6 (GenBank accession no. PP341234, Addgene plasmid ID 216312) was previously described[79].

Bacterial Expression

Nanobodies, NanoBondies, sfGFP and ODC were transformed into competent *E. coli* BL21 DE3 cells (Agilent). Transformed cells were grown on LB Agar plates with 50 µg/mL kanamycin for 16 h at 37 ºC. A single colony was picked from the plate and used to inoculate 10 mL LB medium containing 50 µg/mL kanamycin. This starter culture was incubated at 37 ºC with shaking at 200 rpm for 16 h or until turbid (4 h). The starter culture was then used to inoculate 1 L of LB with 50 µg/mL kanamycin. The 1 L culture was incubated at 37 ºC with 200 rpm shaking. When OD_{600} reached 0.5-0.6, expression was induced with 0.42 mM isopropyl β-D-1-thiogalactopyranoside (IPTG) for 16 h at 18 ºC with 200 rpm shaking. Bacteria were pelleted by centrifugation at 4,000 g.

Mammalian Expression

mCD45d1d2, CD45d1d2, CD45d and CD45d mutants were expressed in Expi293F cells (Gibco). Expi293F cells were grown in Expi293F media (Gibco) under 80% humidity and 8% (v/v) CO_2 at 37 ºC at 95 rpm. Transfections were conducted according to manufacturer's recommendations using the Expi293F Transfection kit (Gibco). Briefly, Expi293F cells were brought to 3.0×10^6 cells/mL. 1 µg of plasmid DNA per mL of cell culture was incubated with Expifectamine reagent for 20 min at 25 °C. This plasmid-liposome mixture was then added dropwise to the prepared Expi293F cells, and the cell culture was returned to the incubator. 18-22 h following transfection, Expifectamine Transfection Enhancers 1 and 2 were added to the cell flask. On day 5 following enhancer addition, cells were pelleted by centrifugation at 300 g, and the supernatant was collected. The supernatant was spun again at 4,000 g, then sequentially syringe-filtered through 0.45 µm and 0.22 µm filters (Starlab).

C-tag purification

NanoBondies and ODC bait protein were purified via C-tag affinity purification. One pellet corresponding to 1 L of bacterial culture was resuspended in lysis buffer: 20 mM Tris-HCl, 150 mM NaCl at pH 7.4, supplemented with 4 mM ethylene glycol-bis(β-aminoethyl ether)-N,N,N′,N′-tetraacetic acid (EGTA), 0.1 mg/mL lysozyme, 1 mg/mL cOmplete mini EDTA-free protease inhibitor (Sigma-Aldrich) and 1 mM phenylmethanesulfonyl fluoride (PMSF). The resuspended pellet was then sonicated on ice for 1 min at 30% amplitude, with pulses of 1 s on and 1 s off. The pellet was allowed to rest on ice for 1 min, then the sonication and rest step were repeated 3 more times. The lysate was then spun at 30,000 g and the cleared lysate was collected. An Econo-PAC Chromatography Column (Bio-Rad) containing 1 mL of Capture Select C-tag XL Affinity Matrix (Thermo Fisher Scientific) was equilibrated by 2×10 column volume (CV) washes in C-tag wash buffer (20 mM Tris-HCl, 150 mM NaCl at pH 7.4). Cleared lysate was added to the column with equilibrated resin. Lysate was incubated with resin for 1 h at 4 ºC with end-over-end rotation. The resin was then washed twice with wash buffer (20 mM Tris-HCl, 150 mM NaCl, 4 mM EGTA, pH 7.4). Protein was eluted using 6 × 1 CV washes of elution buffer: 20 mM Tris-HCl, 1 M NaCl, 50% (v/v) propylene glycol and 2 mM EGTA. The amount of protein was evaluated by A_{280}. Extinction coefficients were based on ExPASy ProtParam[80].

Pooled elutions were dialyzed in 3.5 kDa molecular weight cut-off Spectra/Por tubing (Spectrum Labs) overnight at 4 ºC at 1,000-fold excess against TBS (20 mM Tris-HCl, 150 mM NaCl, pH 7.4) with 100 µM EGTA. This dialysis was repeated once more for 3 h. The pooled elutions were then dialyzed for a further 3 h against a 1,000-fold excess of HBS (50 mM HEPES, 150 mM NaCl, pH 7.4) with 100 µM EGTA. Dialyzed protein was concentrated using a 10 kDa molecular weight cut-off spin concentrator (Vivaspin). Protein was stored in aliquots at -80 ºC to minimize freeze-thawing. Protein concentrations were determined using A_{280}. Typical yield was 1 mg per L of culture for NanoBondies.

SpySwitch purification of SpyTag003-tagged nanobodies

Nanobody cell pellets were prepared as above but were resuspended in 1× SpySwitch buffer (50 mM Tris-HCl pH 7.5, 300 mM NaCl). The SpySwitch purification protocol has been described[81]. Briefly, SpySwitch resin (0.75-1 mL per 1 L bacterial culture) was equilibrated with 2×10 CV SpySwitch buffer in an Econo-PAC Chromatography Column (Bio-Rad). Clarified cell lysate was added to the equilibrated resin and incubated for 1 h at 4 ºC with end-over-end rotation. Supernatant was allowed to flow through by gravity. The resin was washed with 2× 10 CV SpySwitch buffer. For nanobody purification, pH-dependent elution was employed. 6× 1.5 CV of SpySwitch pH elution buffer (50 mM acetic acid, 150 mM NaCl, pH 5.0) was incubated with the resin for 5 min per elution. Elutions were collected into neutralization buffer (0.3 CV of 1 M Tris-HCl pH 8.0). Proteins were dialyzed as above, into TBS. Approximate yield for nanobodies was 1-2 mg per L of culture.

Ni-NTA purification

CD45d1d2, CD45d (CD45d1d2-MBP), CD45d binding site mutants, SpyTag003-sfGFP and SpyCatcher002-MBP were purified by nickel-nitrilotriacetic acid (Ni-NTA) affinity chromatography. Mammalian cell supernatant was collected and prepared as outlined above. The supernatants were supplemented with 10× Ni-NTA buffer (500 mM Tris-HCl, 3 M NaCl, pH 7.8) at 10% (v/v). 1 mL of Ni-NTA agarose (Qiagen) was packed in an Econo-PAC Chromatography Column (Bio-Rad). The packed resin was equilibrated with 2 × 10 CV of Ni-NTA buffer (50 mM Tris-HCl, 300 mM NaCl, pH 7.8). Prepared mammalian supernatant was then added to the equilibrated resin and incubated for 1 h at 4 ºC with end-over-end rotation. Supernatant was allowed to flow through by gravity. The resin was then washed with 2× 10 CV of Ni-NTA wash buffer (10 mM imidazole in Ni-NTA buffer). Protein was eluted by 6× 1 CV of elution buffer (200 mM imidazole in Ni-NTA buffer). Protein was dialyzed as described for NanoBondies, twice with TBS and once with HBS. Approximate yield for CD45d is 88 mg per L culture. Approximate yield for hCD45d1d2 is 13 mg per L culture. hCD45d1d2 was biotinylated as described[82].

NanoBondy-His_6 and DuoBondies were purified using cOmplete His-Tag purification resin (Roche). Bacterial cell pellets were lysed and prepared as above but were resuspended in sodium phosphate buffer (50 mM NaH_2PO_4, 300 mM NaCl, pH 8.0) supplemented with 2 mM EGTA and 5 mM imidazole. 1 mL cOmplete His-Tag agarose (Roche) was packed in an Econo-PAC Chromatography Column (Bio-Rad). The packed resin was then equilibrated with 2× 10 CV of sodium phosphate buffer. Prepared bacterial lysates were added to the equilibrated resin and incubated for 1 h at 4 ºC with end-over-end rotation. Supernatant was allowed to flow through by gravity. The resin was washed with 2× 10 CV of wash buffer (50 mM NaH_2PO_4, 300 mM NaCl, 10 mM imidazole, pH 8.0). Protein was eluted by 6× 1 CV elution buffer (50 mM NaH_2PO_4, 300 mM NaCl, 250 mM imidazole, pH 8.0). Protein was dialyzed as described above twice in TBS and once in HBS. Approximate yield for His_6-tagged NanoBondy was 7 mg and for DuoBondies was 1.5-4 mg per L of culture.

Polyacrylamide gel electrophoresis
For protein visualization, samples were mixed with 6× SDS loading buffer [234 mM Tris-HCl pH 6.8, 24% (v/v) glycerol, 120 µM bromophenol blue, 234 mM SDS] and 50 mM dithiothreitol (DTT) and heated at 99 °C for 3 min. Unless otherwise specified, SDS-PAGE was performed using 12-16% (w/v) polyacrylamide gels at 180 V in SDS-PAGE buffer [25 mM Tris-HCl, 192 mM glycine, 0.1% (w/v) SDS] in either an XCell SureLock system (Thermo Fisher) or a Mini Gel Tank (Invitrogen). Gels were washed twice with distilled water, then stained with Brilliant Blue G-250. Gels were destained in distilled water and imaged using an iBright FL1500 imaging system (Thermo Fisher), with analysis using iBright Analysis software versions 5.01 or 5.2.0 (Thermo Fisher).

Size-exclusion Chromatography
C-tag or His-Tag purified proteins were injected onto a pre-equilibrated Hi-Load 16/600 Superdex 200 pg column (GE Healthcare). Samples were run on an ÄKTA Pure 25 (GE Healthcare) fast protein liquid chromatography machine at 4 ºC into HBS + 100 µM EGTA, pH 7.4. Elutions were monitored by absorbance at 230 nm, 260 nm and 280 nm. Peak analysis was conducted using SDS-PAGE and desired fractions were concentrated at 4 ºC using a 10 kDa molecular weight cut-off spin concentrator (Vivaspin). Proteins were stored at -80 ºC.

PNGase F expression and digestion
pOPH6, a kind gift from Shaun Lott (Addgene plasmid ID 40315)[83],was transformed into competent *E. coli* BL21 DE3, as described above, and grown on LB Agar plates with 100 µg/mL carbenicillin for 16 h at 37 ºC. Bacterial growth, induction and expression were conducted as above. A bacterial pellet corresponding to 1 L of culture was resuspended in 50 mL ice-cold periplasmic lysis solution (0.5 M sucrose, 0.1 M Tris-HCl, 1 mM EDTA, pH 8.0), then pelleted again at 3,000 g for 20 min and the supernatant discarded. The pellet was then resuspended in 50 mL ice-cold MilliQ water and incubated for 10 min on ice. To the resuspended pellet was added $MgCl_2$ to a final 1 mM and the mixture was incubated on ice for a further 10 min. The bacteria were pelleted again at 3,000 g for 20 min and the supernatant retained. This supernatant was supplemented with 10× Ni-NTA buffer (500 mM Tris-HCl, 3 M NaCl, pH 7.8) at 10% (v/v). PNGase F was purified using Ni-NTA as described above. Size-exclusion chromatography was used as a secondary purification step as above. PNGase F was obtained at ~11 mg per L of culture. Purified PNGase F was aliquoted and stored at -20 ºC in HBS + 20% (v/v) glycerol.

For digestion, to the reaction mixture was added 10× glycoprotein denaturing buffer (New England Biolabs) at 10% (v/v). Reaction was heated at 100 ºC for 10 min, then centrifuged using a benchtop mini centrifuge at 25 ºC and 2,000 g for 1 min, and cooled on ice for 2 min. To this denatured reaction was added 10× glycoprotein buffer 2 (New England Biolabs) and 10% (v/v) NP-40 (New England Biolabs), both at a final 10% (v/v). MilliQ H_2O was added to reach the desired final volume. Finally, 1 µg of PNGase F was added to each reaction. Digestion was conducted at 37 ºC for 2 h.

ELISA
Nunc MaxiSorp plates (Thermo Fisher) were coated with 80 nM SpyCatcher002-MBP in PBS (137 mM NaCl, 2.7 mM KCl, 10 mM Na_2HPO_4 and 1.8 mM KH_2PO_4, pH 7.4) and incubated for 16 h at 4 ºC. Plates were washed 3 times with TBS-T [TBS + 0.1% (v/v) Tween-20], with a 5 min incubation for each wash. Plates were blocked for 1 h at 25 °C in blocking buffer: 1% (w/v) bovine serum albumin (BSA) (Sigma-Aldrich) in TBS-T. SpyTag003-fused nanobodies were added to the blocked plates at a final 80 nM in TBS and incubated for 1 h at 25 °C. Plates were washed 3 times with TBS-T for 5 min per wash. CD45d1d2-biotin was added to the plates

in 10-fold serial dilutions in TBS and incubated for 1 h at 25 °C. Plates were washed 3 more times with TBS-T, incubating for 5 min per wash. Pierce High Sensitivity Streptavidin-horseradish peroxidase (HRP) (Thermo Fisher) diluted to 0.2 µg/mL in blocking buffer was added to the plates and incubated for 1 h at 25 °C. The plates were washed 6 times with TBS-T, with 5 min per wash. Plates were incubated at 25 ºC with 1-step Ultra TMB-ELISA Substrate Solution (Thermo Scientific). The reaction was stopped at the 2 min time-point by the addition of 1 M HCl.

For ELISA in Figure S5C, a Nunc MaxiSorp plate was coated with 80 nM of CD45d variants (WT, E105R or I104R) in PBS and incubated for 16 h at 4 ºC. Plates were washed 3 times with TBS-T, with a 5 min incubation for each wash. Plates were blocked for 1 h at 25 °C in blocking buffer: 1% (w/v) BSA (Sigma-Aldrich) in TBS-T. 2H5 R72C NanoBondy was added to the plates in 10-fold serial dilutions in TBS and incubated for 1 h at 25 °C. Plates were washed 3 more times with TBS-T, incubating 5 min per wash. MonoRab anti-VHH HRP (GenScript, A01861) diluted to 0.2 µg/mL in blocking buffer was added to the plates and incubated for 1 h at 25 °C. The plates were washed 6 times with TBS-T, with 5 min per wash. Plates were incubated at 25 ºC with 1-step Ultra TMB-ELISA Substrate Solution (Thermo Fisher). The reaction was stopped at the 2 min time-point by the addition of 1 M HCl.

Absorbance measurements were collected at 450 nm (A_{450}) using a FLUOstar Omega plate reader (BMG Labtech) and Omega MARS software. Binding curves were visualized by GraphPad PRISM software (version 10.1.1).

Cell culture for immortalized cell lines

Expi293F cells were from Thermo Fisher. YTS cells (RRID:CVCL_D324) and NK92 cells (RRID:CVCL_2142)[84] were a kind gift from Daniel Davis (Imperial College London). Expi293F cells were grown in Expi293 media (Thermo Fisher) at 37 ºC, 80% humidity and 8% (v/v) CO_2 with shaking according to manufacturer's guidelines. YTS cells were grown in Roswell Park Memorial Institute 1640 (RPMI-1640) supplemented with 10% (v/v) fetal bovine serum (FBS), 2 mM L-glutamine, 10 mM HEPES, 1 mM sodium pyruvate, 4.5 g/L glucose and 1.5 g/L sodium bicarbonate. NK92 cells were grown in Minimum Essential Medium Alpha (MEM-Alpha) supplemented with 10% (v/v) FBS, 10% (v/v) horse serum, 50 mM 2-mercaptoethanol, 2 mM GlutaMAX, and 200 U/mL rhIL-2 (PeproTech). YTS and NK92 cells were grown at 37 ºC and 5% (v/v) CO_2. Cells were passaged at 70-80% confluency. Cells were sub-cultured for less than 3 months. Cells were validated as mycoplasma-negative by PCR.

Flow Cytometry for Nanobody binding

YTS, NK92 and Expi293F cells were washed in PBS and seeded at 1 million cells/well of a 96 well CELLSTAR V-bottom plate (Greiner). Cells were incubated with 2 µM purified nanobody or 1 µg/mL anti-human CD45 antibody (Invitrogen, clone HI30) in flow buffer [PBS + 1% (w/v) BSA] for 1 h at 25 °C. Cells were washed 3 times in PBS by centrifugation at 150 g at 4 ºC for 3 min. Cells were then incubated with secondary antibody in flow buffer for 1 h at 25 °C. For samples incubated with mouse anti-human CD45, the secondary antibody was polyclonal Alexa Fluor 647-conjugated, highly cross-adsorbed goat anti-mouse IgG (Invitrogen, RRID AB_2535805), at 4 µg/mL in flow buffer at 25 ºC. For samples incubated with nanobody, the secondary antibody was iFluor647-conjugated MonoRab rabbit anti-camelid VHH antibody (GenScript) at 1 µg/mL in flow buffer at 25 ºC. Cells were washed 4 times at 4 ºC. Cells were then resuspended in LIVE/DEAD Fixable Aqua (Invitrogen) at 1 µL reconstituted stain per 1 million cells and incubated for 30 min at 25 °C in the dark. Cells were washed with PBS, then resuspended in PBS. To the resuspended cells was added an equal volume of 4% (w/v) paraformaldehyde in PBS, for a final concentration of 2% (w/v) for 20 min at 25 ºC. To these fixed cells was added PBS. Cells were then centrifuged, washed once

in flow buffer, then resuspended in fresh flow cytometry buffer at 25 ºC. Samples were immediately analyzed on a CytoFlex LX analyzer. Compensation was conducted at the start of each analysis. Data were collected using CytExpert version 2.5 and analyzed using FlowJo version 10.1.0. Events were gated on cells, singlets, then live cells prior to binding analysis.

Protein conjugation assays

Reactions were carried out in HBS at 37 °C. In cases of hydroxylamine block, reactions were carried out in HBS + 15 mM hydroxylamine (Sigma-Aldrich) at 37 °C. NanoBondy and CD45d were mixed in HBS at 10.5 µM each. Reaction was started by addition of 2 mM $CaCl_2$, with 2 mM EGTA pH 8.0 added to 'no calcium' controls. Reactions were incubated for 1 h, then quenched by addition of 10× glycoprotein denaturing buffer (New England Biolabs) at 10% (v/v). Reactions were PNGase F-digested as described above, then visualized by SDS-PAGE with Coomassie staining. Crosslinking between proteins at different sites leads to different polypeptide chain organizations with distinct gel mobility, as previously shown[78].

Protein conjugation time-courses

Unless otherwise specified, reactions were carried out in HBS pH 7.4 at 37 °C. To measure pH-dependence, HBS was supplemented with 50 mM MES to buffer across the desired pH range. To measure buffer-dependence, reactions were also carried out in TBS pH 7.4 at 37 °C. For both pH- and buffer-dependency experiments, proteins were buffer-exchanged into the desired buffer using a Vivaspin 500 10 kDa MWCO spin concentrator (Vivaspin) prior to assembling reactions.

A reaction mix was assembled by adding NanoBondy and CD45d at 10.5 µM in the desired buffer. Reaction was held at the desired temperature and initiated with 2 mM $CaCl_2$. At each timepoint, a fraction of the reaction mix was removed and quenched by addition of 4× stop buffer (60 mM EGTA and 4× glycoprotein denaturing buffer) for a final EGTA concentration of 15 mM and final protein concentrations of 10 µM. Quenched reactions were immediately heated at 100 °C for 10 min. For the 0 min timepoint, stop buffer was added first, followed by 2 mM $CaCl_2$. Reactions were PNGase F-digested as described above, then visualized by SDS-PAGE with Coomassie staining. Protein concentration following PNGase F-digestion was 5 µM.

Quantification of protein conjugation using gel densitometry

Quantification of band intensity for SDS-PAGE was conducted using iBright Analysis software (Thermo Fisher, version 5.4.0) with rolling ball correction. Relative intensity of each product band was calculated by the iBright software by determining the ratio of the intensity of the product band (e.g. NanoBondy:CD45d) to the intensity of the NanoBondy-SPM band from the calcium-free lane:

$$\text{Relative intensity}_{\text{NanoBondy:CD45d}} = \frac{\text{Intensity}_{\text{NanoBondy:CD45d}}}{\text{Intensity}_{\text{NanoBondy-S}}}$$

For lanes with multiple product bands, the relative intensity of each band was independently determined and then summed. To determine % NanoBondy coupled, molecular weight correction was applied:

$$\%\ \text{NanoBondy coupled} = \text{Relative intensity}_{\text{NanoBondy:CD45d}} \times \frac{\text{Molecular Weight}_{\text{NanoBondy-SP}}}{\text{Molecular Weight}_{\text{NanoBondy:CD45d}}} \times 100$$

For conditions where the software failed to detect a product band, % NanoBondy conjugated was set to 0.

Quantification of band intensity for Western blots in Figure 7A and 7B was conducted using iBright Analysis software (Thermo Fisher, version 5.4.0) with rolling ball correction. Quantification of band intensity for Figure 7C was conducted using Image Lab software (Bio-Rad, version 6.1.0). For Figures 7A and 7C, the uncleaved NanoBondy-SPM band was used

as the reference band. For Figure 7B, the CD45 band population without calcium addition was used as the reference band. For Figure 7B, band boundaries were manually set. For Figures 7A and 7C, bands were automatically detected. No molecular weight correction was performed for Western blot quantification, since detection was based on antibody recognition.

For Figures 7A and 7C, % NanoBondy coupled was calculated by determining the ratio of the intensity of the product band (NanoBondy:CD45) to the intensity of the NanoBondy-SPM band from the calcium-free lane:

$$\%\ \text{NanoBondy coupled} = \frac{\text{Intensity}_{\text{NanoBondy:CD45}}}{\text{Intensity}_{\text{NanoBondy-SPM}}} \times 100$$

For Figure 7B, % CD45 conjugated was calculated by determining the ratio of the intensity of the product band (NanoBondy:CD45) to the intensity of the major CD45 band from the calcium-free lane.

$$\%\ \text{CD45 coupled} = \frac{\text{Intensity}_{\text{NanoBondy:CD45}}}{\text{Intensity}_{\text{CD45}}} \times 100$$

Intact protein ESI Mass Spectrometry

For intact protein MS on anti-CD45 2H5 R72C NanoBondy-His_6, a RapidFire 365 platform (Agilent) was used. The Rapid365 platform consisted of a jet-stream electrospray ionization source coupled to a 6550 Accurate-Mass Quadrupole Time-of-Flight (Q-TOF) (Agilent). 5 µM of 2H5 NanoBondy in HBS was diluted 1:1 with water before formic acid was added to a final concentration of 0.9% (v/v). The protein sample was aspirated under vacuum for 0.3 s and loaded onto a C4 solid-phase extraction cartridge. Washes were conducted using 0.1% (v/v) formic acid in water for 5.5 s. The sample was then eluted onto the Q-TOF detector for 5.5 s. MassHunter Qualitative Analysis B.07.00 (Agilent) was used for data analysis. Expected protein molecular weight was calculated using the ExPASy ProtParam tool[80], with 2 Da subtracted to account for the formation of a disulfide bond[85].

Crosslinking MS sample preparation

The reaction mix was assembled by adding 2H5 R72C NanoBondy to CD45d in HBS to final protein concentrations of 10.5 µM NanoBondy and 10.5 µM CD45d. The total mass of protein in the reaction was 1 mg. Reaction was initiated with 2 mM $CaCl_2$ and held at 37 ºC for 2 h. Reaction was PNGase F-digested as described above. PNGase F was heat-inactivated by holding the reaction at 75 ºC for 10 min. Reaction mix was transferred to -20 ºC for overnight storage and transported to mass spectrometry analysis on dry ice.

An equal volume of 5% (w/v) SDS with 100 mM Tris-HCl (pH 8.5) was added to 500 µg calcium-cleaved 2H5 R72C NanoBondy:CD45d conjugate, before the sample was incubated at 99 ºC for 10 min, followed by water bath sonication (Fisherbrand, FB11203) at 37 kHz, power 100, at 25 ºC on sweep mode for a further 10 min. Ammonium bicarbonate (pH 8.5) was added to a final 50 mM, before addition of DTT to a final 8 mM, followed by incubation at 37 ºC for 30 min. Iodoacetamide was then added to a final 20 mM and incubated for 30 min in darkness at 25 ºC before adding trypsin (Trypsin Gold, Promega) at a ratio of 50:1 analyte:trypsin, followed by overnight incubation at 37 ºC with shaking. Digestion was quenched with a final trifluoroacetic acid concentration of 0.5% (v/v), before desalting using Waters Oasis HLB Solid Phase Extraction (SPE) plate. Samples were then reconstituted in Buffer A (100 µL 10 mM ammonium formate, pH 10.0), before fractionation (ACQUITY UPLC BEH C18 VanGuard Pre-column 130Å, 1.7 µm, 2.1 mm × 5 mm) using a gradient of 4% to 35% Buffer B [80% (v/v) acetonitrile, 10 mM ammonium formate, pH 10.0] over 8 min with fractions collected every 20 s. Fractions were then pooled to a total of 8 fractions and each fraction was reconstituted in 0.1% (v/v) formic acid before LC-MS/MS.

LC-MS/MS (Crosslinking Mass Spectrometry)

An UltiMate 3000 RSLCnano liquid chromatography system (Thermo Fisher), with 50 cm µPAC Neo HPLC analytical column and 0.075 mm × 20 mm trap cartridge (Acclaim PepMap C18 100 Å, 3 µm) was connected to an Orbitrap Eclipse Tribrid mass spectrometer (Thermo Fisher) via a SilicaTip emitter. Column temperature was set to 45 ºC, with an analytical column flow rate of 750 nL/min. Mobile phase A was 0.1% (v/v) formic acid with 3.2% (v/v) acetonitrile and mobile phase B was 0.1% (v/v) formic acid with 96.8% (v/v) acetonitrile. An elution gradient from 3% to 55% mobile phase B over 48 min was applied, with a total run time of 60 min. The Orbitrap Eclipse Tribrid mass spectrometer was externally calibrated using Pierce FlexMix calibration solution and nano-ESI was performed using a SilicaTip emitter, connected to the LC *via* an HPLC liquid junction tee.

Spray stability and signal intensity were optimized by varying the SilicaTip electrospray to a final positive ion voltage of 2,000 V and modifying the Silica Tip positioning in the *x*, *y* and *z* dimensions. Transfer capillary temperature was set to 275 ºC, RF lens was set to 40%, precursor ion mass resolution was set to 120,000, precursor ion mass range was set to 350 -2000 *m/z* and precursor ion charge state was set from 3^+ to 7^+. MS^1 spectra were acquired with a Data-Dependent Analysis duty cycle (Top20), automatic gain control (AGC) was set to target 400,000 (100%), maximum injection time mode was set to Auto, precursor ions were isolated with a 1.4 *m/z* window using a quadrupole mass filter, and monoisotopic precursor selection was set to peptide peak determination. For Orbitrap MS^2 acquisition using Higher energy Collision-induced Dissociation (HCD), collision energy was set to 30%, resolution was set to 30,000, mass range was set to normal, AGC was set to normal with an absolute AGC value of 5.00×10^4 and maximum injection time mode was set to Auto.

The samples were run in technical triplicate and RAW files were processed using Proteome Discoverer 2.5 (Thermo Fisher) with the Sequest HT[86] database searching node and the XlinkX[87] crosslink processing node. For Sequest HT, dynamic modifications included: oxidation (+15.995 Da, M) and N-terminal acetylation (+42.011 Da). Static modifications included: carbamidomethyl (+57.021 Da, C) with false discovery rate (FDR) set to 0.01 using the Target Decoy PSM Validator node. The FASTA file database contained sequences for 2H5 R72C NanoBondy, CD45d, PNGase F and 200 randomly selected decoy proteins for false discovery analysis. For crosslink identification, the FASTA file contained 2H5 R72C NanoBondy , CD45d and PNGase F. Relative to the FASTA file amino acid sequence, aspartic acid and lysine/threonine/serine/arginine/tyrosine/α-amino sites were considered to crosslink with an overall chemical difference of O(-1)H(-1) from the peptides off the initial proteins 2H5 R72C NanoBondy and CD45d to the crosslinked entity, corresponding to a zero length crosslinker average mass of -17.0073 Da and a monoisotopic mass of -17.00274 Da. Crosslink residues were selected as: D-K, D-T, D-S, D-R, D-Y and D-α-amino. XlinkX acquisition strategy was set to Noncleavable_fast and minimum signal/noise: 1.5. FDR was set to 0.05 in the XlinkX PD Validator node. Only high confidence crosslinks from D173 of 2H5 R72C NanoBondy were considered for further analysis and all identified crosslinks were manually verified from their corresponding MS/MS fragmentation spectra. The number of crosslinked spectral matches was reported by XlinkX, with the corresponding scan number used to manually annotate the MS/MS spectra from within the RAW file. All data are available on PRIDE (accession number PXD063277) and all validated crosslinks are provided in the Supplementary Information.

Western blotting

YTS cells were seeded at 1.5 million cells/well of a CELLSTAR 96 well V-bottom plate (Greiner). $CD8^+$ T cells were seeded in 15 mL falcon tubes at 4 million cells/condition. Cells were washed twice with HBS at 25 ºC. Washed cells were resuspended with 5 µM NanoBondy

in HBS with or without 5 mM hydroxylamine, or with 1 μM DuoBondy (WT) or DuoBondy (DA) in HBS + 1.5% (w/v) BSA. Reaction was initiated by addition of 2 mM $CaCl_2$, with 2 mM EGTA added to 'no calcium' controls. Cells were incubated at 37 °C for 1 h for NanoBondy assays or 37 ºC for 40 min for DuoBondy assays. Cells were then washed once in HBS at 25 ºC. For lysis, cells were resuspended in 180 μL/million cells ice-cold RIPA buffer [20 mM Tris-HCl, 150 mM NaCl, 1% (v/v) Triton X-100, 0.5% (w/v) sodium deoxycholate, 0.1% (w/v) SDS, pH 7.4] freshly supplemented with 1 mM PMSF and 1× cOmplete mini EDTA-free inhibitors (Roche). Resuspended cells were transferred to 1.5 mL microcentrifuge tubes and incubated on ice for 20 min. Lysed cells were then centrifuged at 12,000 g for 20 min at 4 °C to pellet nuclei. Lysate was mixed with 6× SDS loading buffer [234 mM Tris-HCl pH 6.8, 24% (v/v) glycerol, 120 μM bromophenol blue, 234 mM SDS] to a final volume of 1× SDS loading buffer. For anti-VHH visualization, 50 mM DTT was included, whereas for anti-CD45 visualization reducing agent was not used. Lysates were heated at 99 °C for 3 min before loading onto SDS-PAGE. For visualization of NanoBondy conjugation products, samples were loaded onto a 4-12% NuPAGE Bis-Tris gel (Invitrogen) and run in MOPS Buffer (Invitrogen) at 180 V for 1 h using a Mini Gel Tank (Invitrogen). For visualization of DuoBondy conjugation products, samples were loaded onto a 4-12% NuPAGE Bis-Tris gel (Invitrogen) and run in MES Buffer (Invitrogen) at 180 V for 1 h using an XCell SureLock Mini-Cell (Invitrogen). For visualization of CD45, samples were loaded onto a 6% Tris-Acetate gel and run in Tris-glycine buffer [25 mM Tris-HCl, 192 mM glycine, 0.1 % (w/v) SDS] at 180 V for 1 h using a Mini Gel Tank (Invitrogen). Gels were washed in MilliQ water, then soaked in 20% (v/v) ethanol in MilliQ water for 10-20 min with gentle rocking at 25 ºC. Proteins were transferred to Polyvinylidene fluoride (PVDF) membranes using an iBlot2 system (Invitrogen) and iBlot2 PVDF Transfer Stack (Invitrogen). Transfer was conducted at 15 V for 13 min.

For anti-VHH visualization, the blocking buffer was TBS with 5% (w/v) skimmed milk and 0.05% (v/v) Tween-20. For anti-CD45 and anti-GAPDH visualization, the blocking buffer was TBS with 3% (w/v) BSA and 0.05% (v/v) Tween-20. Membranes were blocked at 4 °C for 16 h. Blocked membranes were incubated with primary antibodies for 1 h at 25 °C; mouse anti-human CD45 (Invitrogen clone HI30) at 1 μg/mL or mouse anti-human GAPDH (antibodies.com, clone GA1R) at 2 μg/mL or AffiniPure goat anti-alpaca IgG VHH domain (Jackson ImmunoResearch, RRID AB_2810907) at 0.6 μg/mL. Membranes were washed 3 times with TBS + 0.05% (v/v) Tween-20, incubating 3 min per wash at 25 ºC. Membranes were then incubated with secondary stain for 1 h at 25 °C. For anti-CD45 and anti-GAPDH visualization, the secondary antibody was anti-mouse IgG peroxidase antibody (Sigma-Aldrich) at 1:2,500 in blocking buffer. For anti-VHH, the secondary antibody was rabbit anti-goat IgG HRP (Invitrogen, RRID AB_2534006) at 0.2 μg/mL dilution in blocking buffer. Membranes were then washed 3 times in TBS-T, incubating 3 min per wash at 25 ºC. Blots were visualized by SuperSignal West Pico PLUS Chemiluminescent Substrate (Thermo Fisher) using an iBright FL1500 imaging system (Thermo Fisher).

Primary $CD8^+$ T cell isolation and transduction

Human $CD8^+$ T cells were isolated from leukocyte cones using negative selection. Blood samples were incubated with 150 μL Rosette-Sep Human $CD8^+$ enrichment cocktail (STEMCELL Technologies) per mL of blood for 20 min at 25 ºC. The blood:enrichment cocktail mixture was diluted 2:1 with PBS and layered on top of Ficoll Paque Plus (GE) at a ratio of 0.8 Ficoll to 1.0 blood mixture. Falcon tubes containing the layered preparation were centrifuged at 1,200 g for 20 min at 25 ºC with slow acceleration and deceleration. The resulting buffy coat, containing isolated $CD8^+$ T cells, was collected. Cells were counted, then resuspended at 1 million cells/mL in complete RPMI: RPMI + 10% (v/v) FBS and 100 U/mL penicillin/streptomycin with 50 U/mL IL-2 (PeproTech) and CD3/CD28 human T-activator

DynaBeads (Thermo Fisher) at a 1:1 bead to cell ratio. Isolated $CD8^+$ human T cells were cultured at 37 ºC and 5% (v/v) CO_2.

Confocal microscopy to evaluate NanoBondy cell-surface labeling

Primary human $CD8^+$ T cells were isolated and expanded as in the previous section. $CD8^+$ T cells or Expi293F cells were washed once in HBS, then seeded at 200,000 cells/well of a CELLSTAR 96 well V-bottom plate (Greiner). Cells were stained with 2 μM anti-CD45 NanoBondy (2H5 R72C with 9 residue linker) in HBS with 1% (w/v) BSA and 100 μM EGTA for 1 h at 25 ºC. Cells were then washed 3 times in HBS. Secondary staining was conducted using Alexa Fluor 647-conjugated AffiniPure goat anti-alpaca IgG VHH domain (Jackson ImmunoResearch, RRID AB_2810907) at 0.6 μg/mL in HBS + 1% (w/v) BSA for 40 min at 25 ºC. Cells were then washed 4 times in HBS.

Cells were imaged live on a Zeiss 880 Airyscan laser scanning microscope using a Plan-Apochromat 63× oil immersion objective (Zeiss, NA 1.4) with a pinhole setting of 1 Airy Unit (AU) and a pixel size of 0.1318 μm/pixel. Image acquisitions were controlled by the Zen Black Software. In each region of interest an image was captured by using a solid-state laser with an excitation wavelength of 633 nm, operating with a laser power of 27 μW and a power density 148 mW/cm^2. For every region of interest, a brightfield image was also captured. All imaging was done with a line averaging of 2. The resulting image stacks were handled using Fiji (ImageJ version 1.54p)[88], and the image collage was assembled in Illustrator (Adobe version 29.7.1), presenting a confocal slice. Images for the different samples were collected and processed using the same settings.

Ethics declaration for use of human samples

Leukocyte cones were purchased from the National Health Service's (UK) Blood and Transplantation service (NHS-BT). All cones were anonymized by the NHS-BT before purchase. Ethical approval was provided by the Health Research Authority at National Health Service through a Research Ethics Committee (20/EM/0267) submitted through the Medical Sciences Inter-divisional Research Ethics Committee (IDREC) at the University of Oxford (R51997/RE001). Study samples were obtained by the authority of the institutional board that licensed the use of the material.

Data Analysis and Visualization

Data visualization for ELISA and flow cytometry activation curves was performed using GraphPad Prism 10 (GraphPad Software). Protein structures were visualized using PyMOL version 2.5.4 (Schrödinger). Figures for publication were generated using UCSF ChimeraX version 1.8rc202405230136[89]. NanoBondy structure and docking were predicted using AlphaFold with ColabFold version 1.5.2[90]. To generate AlphaFold2-multimer models of nanobody docking to the extracellular domain of human CD45, an amino acid sequence corresponding to PDB accession code 5FN7 (domains 1 and 2) was used[77]. Figure 2B depicts the CD45 RO isoform, which corresponds to the most abundant CD45 isoform on YTS[91] and activated $CD8^+$ T cells[92].

Safety/hazard statement

Hydroxylamine hydrochloride was handled according to all recommended safety precautions. Dilute solutions for experimental use were prepared within a chemical fume hood. No other unexpected or unusually high safety hazards were encountered during this study.

Data Availability Statement

Plasmids encoding the NanoBondy and CD45d constructs have been deposited in the Addgene repository (https://www.addgene.org/Omer_Dushek/) and sequences of other constructs have been deposited in GenBank as described in the section "Plasmids and cloning". For Crosslinking MS, all validated crosslinks are provided in the Supplementary Information. The MS data that support the findings of this study are openly available in PRIDE at https://www.ebi.ac.uk/pride/, reference number PXD063277. Any requests for further information, or for resources and reagents should be directed to and will be fulfilled by the lead contact, M.R.H..

References

(72) Rokkam, D.; Lupardus, P. J. *Discovery and Characterization of Llama VHH Targeting the RO Form of Human CD45*; preprint; bioRxiv, 2020; p 2020.09.01.278853. https://doi.org/10.1101/2020.09.01.278853.

(73) Keeble, A. H.; Turkki, P.; Stokes, S.; Khairil Anuar, I. N. A.; Rahikainen, R.; Hytönen, V. P.; Howarth, M. Approaching Infinite Affinity through Engineering of Peptide–Protein Interaction. *Proc. Natl. Acad. Sci. U.S.A.* **2019**, *116* (52), 26523–26533. https://doi.org/10.1073/pnas.1909653116.

(74) Huang, J.; Nagy, S. S.; Koide, A.; Rock, R. S.; Koide, S. A Peptide Tag System for Facile Purification and Single-Molecule Immobilization. *Biochemistry* **2009**, *48* (50), 11834–11836. https://doi.org/10.1021/bi901756n.

(75) Pleiner, T.; Bates, M.; Görlich, D. A Toolbox of Anti–Mouse and Anti–Rabbit IgG Secondary Nanobodies. *J. Cell Biol.* **2018**, *217* (3), 1143–1154. https://doi.org/10.1083/jcb.201709115.

(76) Kalinin, R. S.; Ukrainskaya, V. M.; Chumakov, S. P.; Moysenovich, A. M.; Tereshchuk, V. M.; Volkov, D. V.; Pershin, D. S.; Maksimov, E. G.; Zhang, H.; Maschan, M. A.; Rubtsov, Y. P.; Stepanov, A. V. Engineered Removal of PD-1 From the Surface of CD19 CAR-T Cells Results in Increased Activation and Diminished Survival. *Front. Mol. Biosci.* **2021**, *8*, 745286. https://doi.org/10.3389/fmolb.2021.745286.

(77) Chang, V. T.; Fernandes, R. A.; Ganzinger, K. A.; Lee, S. F.; Siebold, C.; McColl, J.; Jönsson, P.; Palayret, M.; Harlos, K.; Coles, C. H.; Jones, E. Y.; Lui, Y.; Huang, E.; Gilbert, R. J. C.; Klenerman, D.; Aricescu, A. R.; Davis, S. J. Initiation of T Cell Signaling by CD45 Segregation at "Close Contacts." *Nat Immunol* **2016**, *17* (5), 574–582. https://doi.org/10.1038/ni.3392.

(78) Scheu, A.; Lim, S. Y. T.; Metzner, F. J.; Mohammed, S.; Howarth, M. NeissLock Provides an Inducible Protein Anhydride for Covalent Targeting of Endogenous Proteins. *Nat Commun* **2021**, *12* (1), 717. https://doi.org/10.1038/s41467-021-20963-5.

(79) Driscoll, C. L.; Keeble, A. H.; Howarth, M. R. SpyMask Enables Combinatorial Assembly of Bispecific Binders. *Nat Commun* **2024**, *15* (1), 2403. https://doi.org/10.1038/s41467-024-46599-9.

(80) Gasteiger, E.; Hoogland, C.; Gattiker, A.; Duvaud, S.; Wilkins, M. R.; Appel, R. D.; Bairoch, A. Protein Identification and Analysis Tools on the Expasy Server. In *The Proteomics Protocols Handbook*; Humana Press, 2005; pp 571–607.

(81) Vester, S. K.; Rahikainen, R.; Khairil Anuar, I. N. A.; Hills, R. A.; Tan, T. K.; Howarth, M. SpySwitch Enables pH- or Heat-Responsive Capture and Release for Plug-and-Display Nanoassembly. *Nat Commun* **2022**, *13* (1), 3714. https://doi.org/10.1038/s41467-022-31193-8.

(82) Fairhead, M.; Howarth, M. Site-Specific Biotinylation of Purified Proteins Using BirA. *Methods Mol Biol* **2015**, *1266*, 171–184. https://doi.org/10.1007/978-1-4939-2272-7_12.

(83) Loo, T.; Patchett, M. L.; Norris, G. E.; Lott, J. S. Using Secretion to Solve a Solubility Problem: High-Yield Expression in Escherichia Coli and Purification of the Bacterial

Glycoamidase PNGase F. *Protein Expression Purif.* **2002**, *24* (1), 90–98. https://doi.org/10.1006/prep.2001.1555.
(84) Gong, J. H.; Maki, G.; Klingemann, H. G. Characterization of a Human Cell Line (NK-92) with Phenotypical and Functional Characteristics of Activated Natural Killer Cells. *Leukemia* **1994**, *8* (4), 652–658.
(85) Klapoetke, S.; Xie, M. H. Disulfide Bond Characterization of Human Factor Xa by Mass Spectrometry through Protein-Level Partial Reduction. *J. Pharm. Biomed. Anal.* **2017**, *132*, 238–246. https://doi.org/10.1016/j.jpba.2016.10.005.
(86) Brodbelt, J. S.; Russell, D. H. Focus on the 20-Year Anniversary of SEQUEST. *J. Am. Soc. Mass Spectrom.* **2015**, *26* (11), 1797–1798. https://doi.org/10.1007/s13361-015-1264-1.
(87) Liu, F.; Lössl, P.; Scheltema, R.; Viner, R.; Heck, A. J. R. Optimized Fragmentation Schemes and Data Analysis Strategies for Proteome-Wide Cross-Link Identification. *Nat Commun* **2017**, *8* (1), 15473. https://doi.org/10.1038/ncomms15473.
(88) Schneider, C. A.; Rasband, W. S.; Eliceiri, K. W. NIH Image to ImageJ: 25 Years of Image Analysis. *Nat Methods* **2012**, *9* (7), 671–675. https://doi.org/10.1038/nmeth.2089.
(89) Meng, E. C.; Goddard, T. D.; Pettersen, E. F.; Couch, G. S.; Pearson, Z. J.; Morris, J. H.; Ferrin, T. E. UCSF ChimeraX: Tools for Structure Building and Analysis. *Protein Sci.* **2023**, *32* (11), e4792. https://doi.org/10.1002/pro.4792.
(90) Mirdita, M.; Schütze, K.; Moriwaki, Y.; Heo, L.; Ovchinnikov, S.; Steinegger, M. ColabFold: Making Protein Folding Accessible to All. *Nat Methods* **2022**, *19* (6), 679–682. https://doi.org/10.1038/s41592-022-01488-1.
(91) Gunesch, J. T.; Angelo, L. S.; Mahapatra, S.; Deering, R. P.; Kowalko, J. E.; Sleiman, P.; Tobias, J. W.; Monaco-Shawver, L.; Orange, J. S.; Mace, E. M. Genome-Wide Analyses and Functional Profiling of Human NK Cell Lines. *Molecular Immunology* **2019**, *115*, 64–75. https://doi.org/10.1016/j.molimm.2018.07.015.
(92) Al Barashdi, M. A.; Ali, A.; McMullin, M. F.; Mills, K. Protein Tyrosine Phosphatase Receptor Type C (PTPRC or CD45). *J Clin Pathol* **2021**, *74* (9), 548–552. https://doi.org/10.1136/jclinpath-2020-206927.

anti-CD45 NanoBondy

Supplementary Figure 1. **Amino acid sequence of lead anti-CD45 NanoBondy (2H5 R72C with 9 residue spacer from clamp site to reactive D).** Residue numbers begin at 1 from the N-terminal methionine, which is cleaved in the final protein sequence.

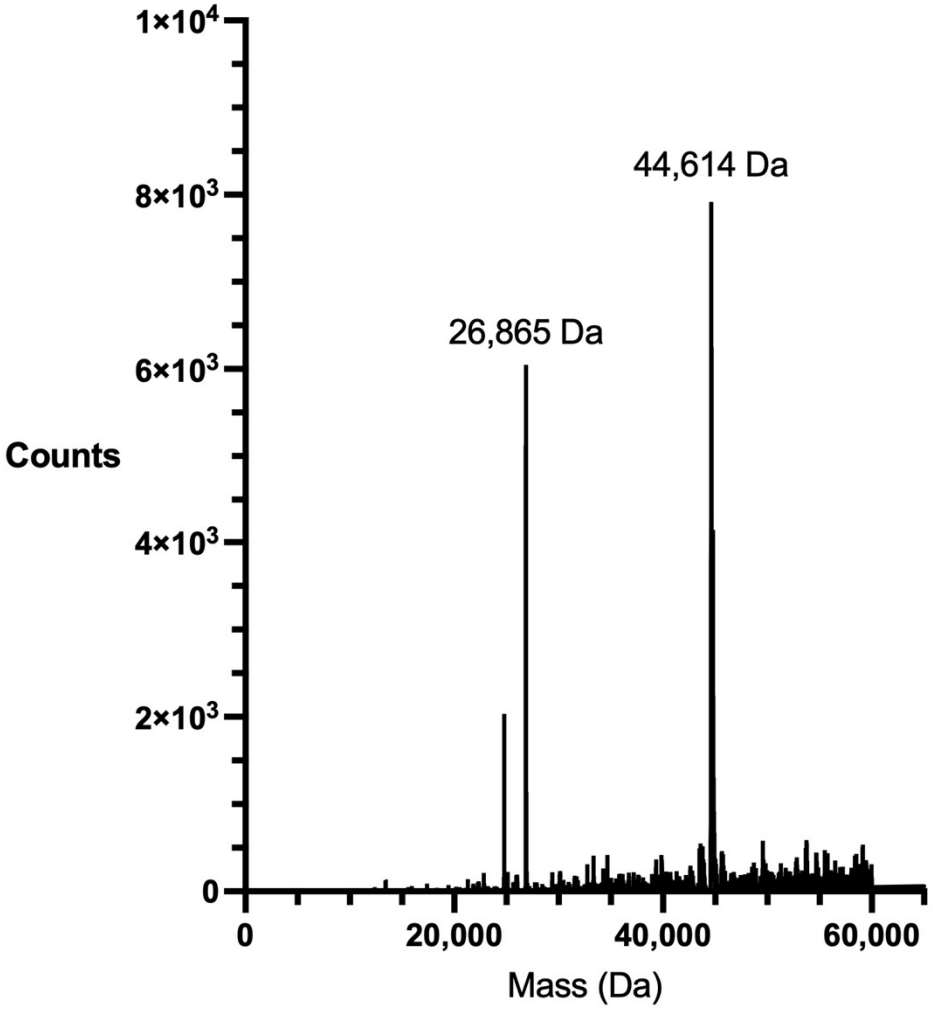

***Supplementary Figure 2*. Intact mass spectrometry of NanoBondy**.
Electrospray ionization mass spectrometry of anti-CD45 2H5 R72C NanoBondy-His_6. Expected mass of the full-length NanoBondy after disulfide formation is 44,614 Da. Expected mass of the SPM cleavage product is 26,865 Da. Representative mass spectrum from two independent experiments.

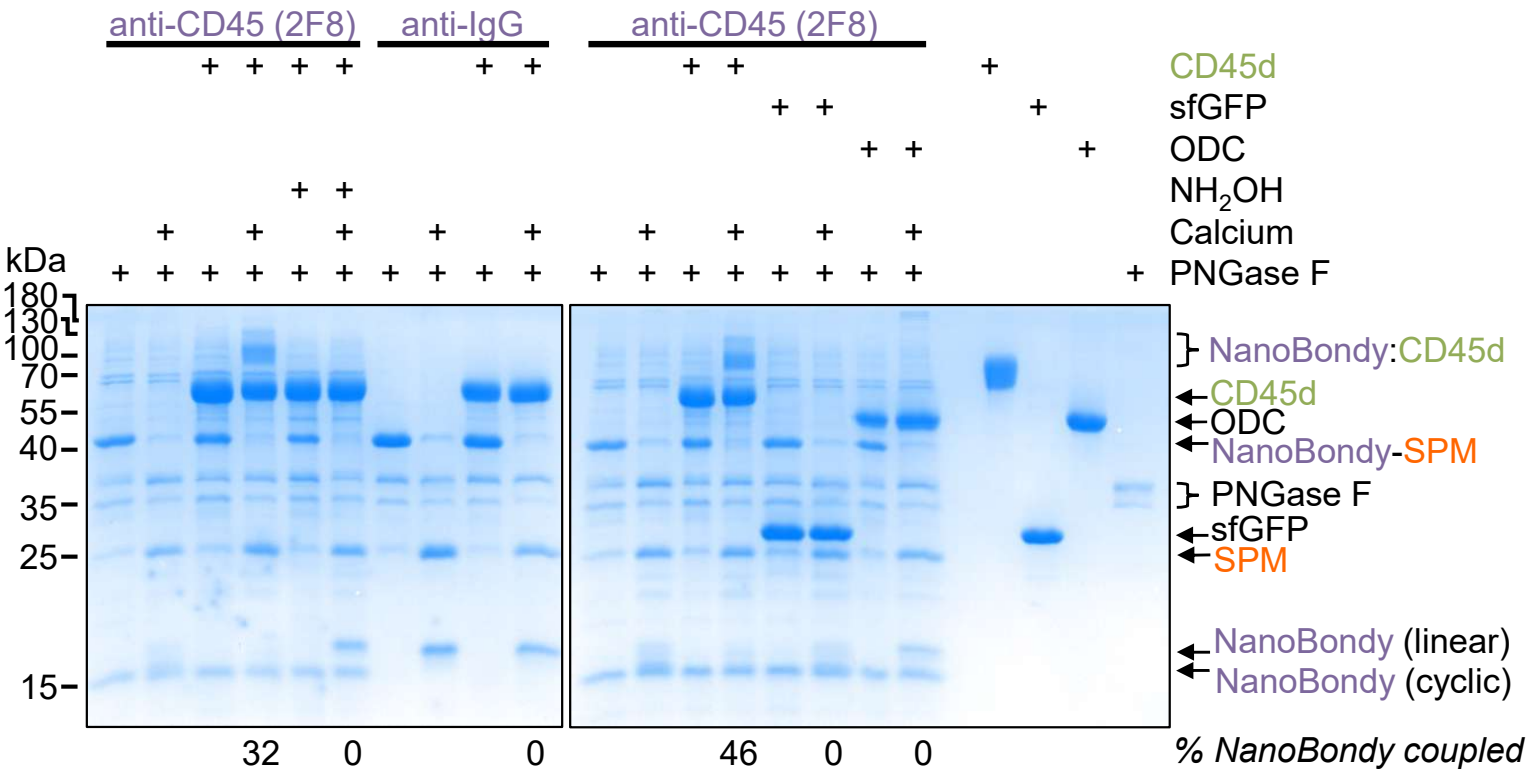

Supplementary Figure 3. **Specificity of 2F8-derived NanoBondy coupling to CD45**. α-CD45 2F8 NanoBondy was incubated ± calcium with CD45d or control proteins ornithine decarboxylase (ODC) or superfolder GFP (sfGFP) for 1 h at 37 ºC in HBS. Hydroxylamine was a competitor. α-IgG NanoBondy was a negative control. Formation of the covalent product was visualized using SDS-PAGE/Coomassie. The experiment was conducted once.

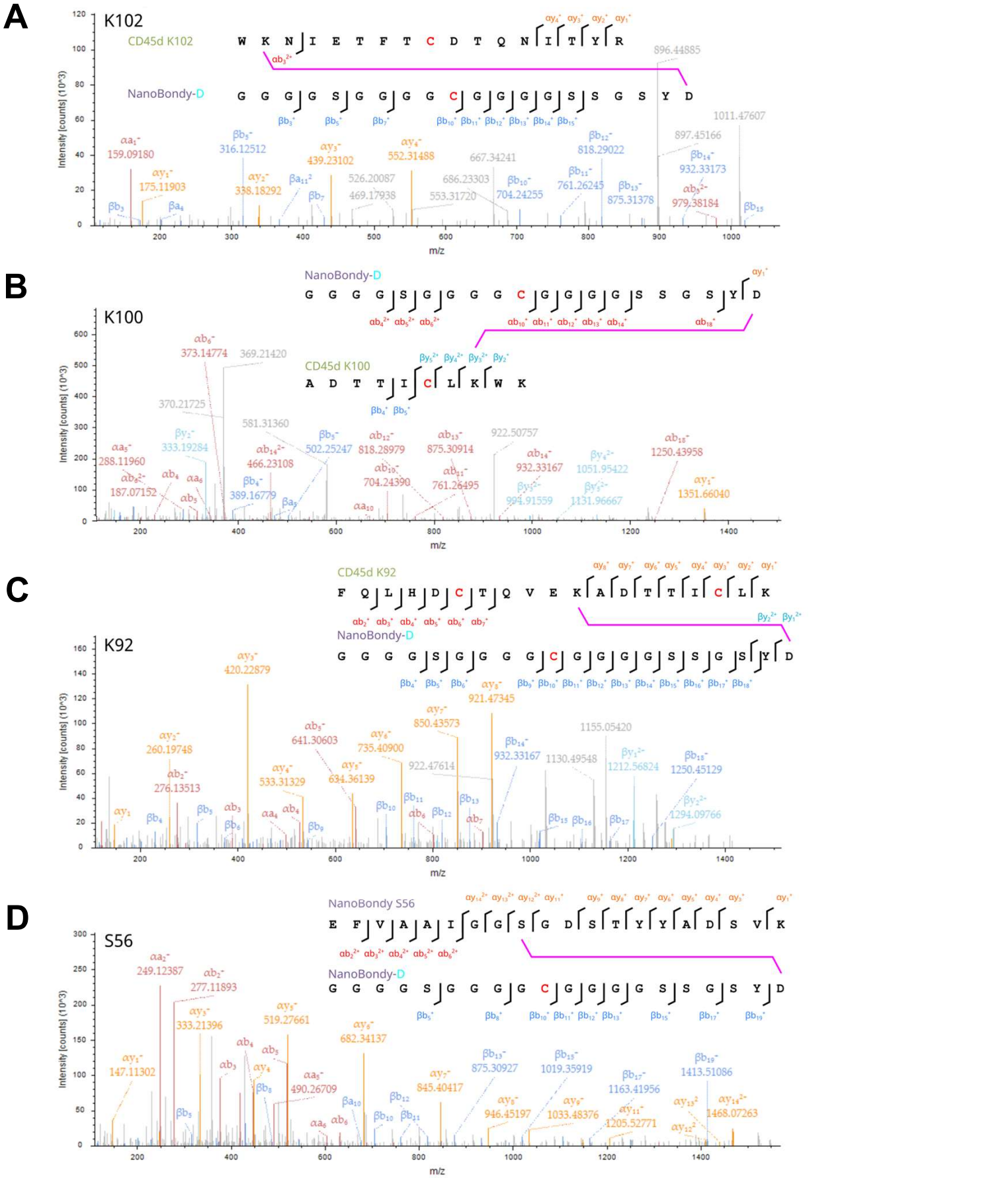

Supplementary Figure 4. **NanoBondy crosslinks mapped in MS/MS.** Higher energy collision-induced dissociation (HCD) fragmentation spectra of identified crosslink precursor ions corresponding to D173 (2H5 R72C NanoBondy) peptide coupled to a CD45d peptide: **(A)** K102, **(B)** K100, **(C)** K92, and self-link corresponding to NanoBondy D173 coupled to **(D)** NanoBondy S56. MS/MS spectra taken directly from Proteome Discoverer. Cysteines are colored red to indicate carbamidomethylation. The two peptides are depicted as α and β peptides (α peptide above β peptide in figure). α-b (red), α-y (orange), β-b (dark blue) and β-y (light blue) ions are marked. Some spectra also contain a ions, which were ignored for fragment annotation. Samples were run in technical triplicate. Deep fractionation MS was conducted once.

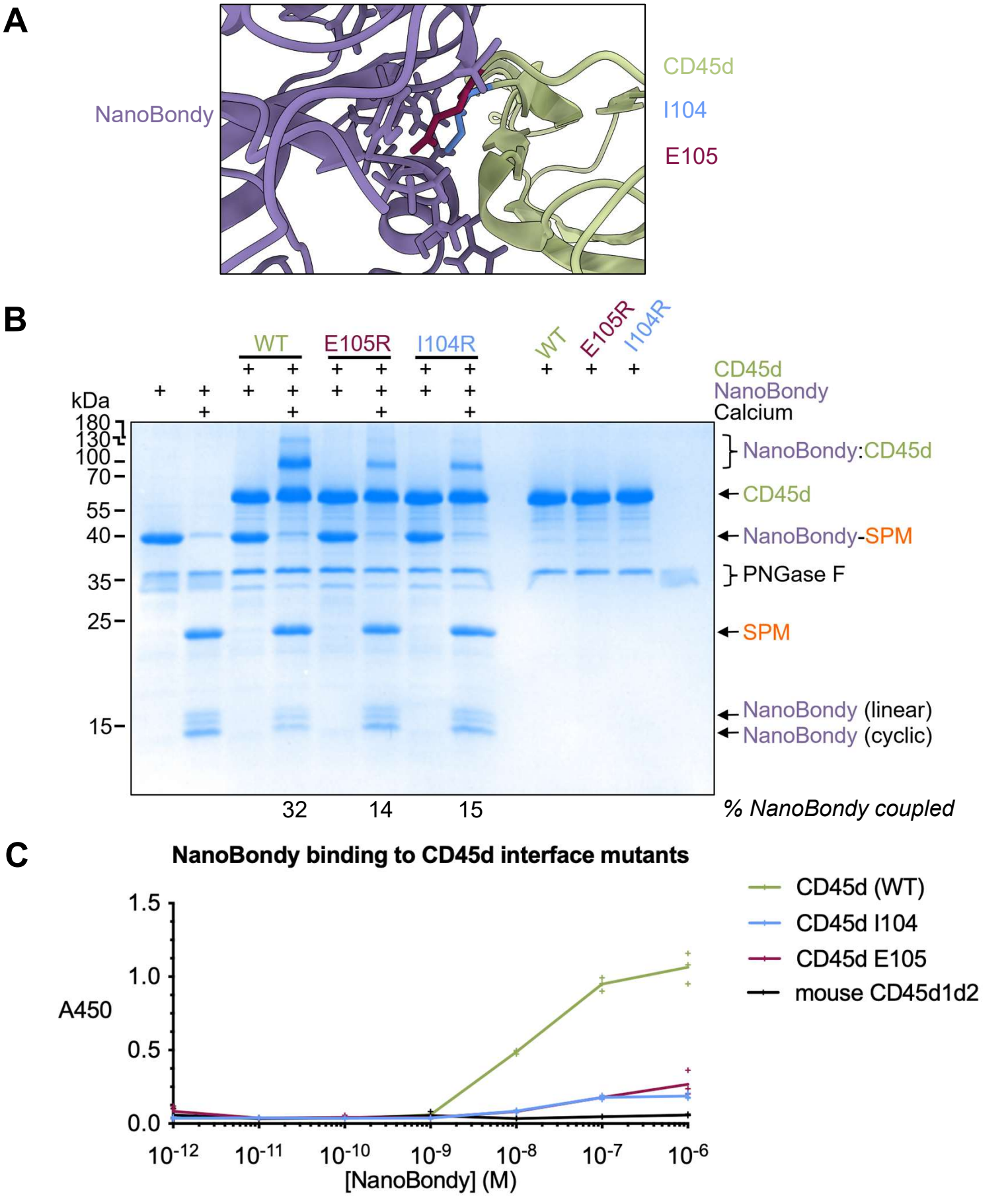

***Supplementary Figure 5*. Validation of predicted NanoBondy docking site on CD45. (A)** AlphaFold2multimer prediction of 2H5 NanoBondy:CD45d docking. E105 (red) and I104 (blue) of CD45 sit at the docking interface. NanoBondy residues 33-36 and 103-107 shown in stick form. **(B)** 2H5 R72C NanoBondy conjugation to CD45d mutants was evaluated by SDS-PAGE/Coomassie. 10.5 µM NanoBondy was incubated with 10.5 µM CD45d variants for 1 h at 37 ºC ± Ca^{2+}, then digested with PNGase F for 2 h. PNGase F was included in all lanes. Representative gel from two independent experiments. **(C)** NanoBondy binding to CD45d mutants evaluated using ELISA. WT CD45d, CD45d mutants, or mouse CD45d (mCD45d1d2, negative control) were bound to the plate and incubated with a titration of NanoBondy variants. NanoBondy binding was detected using anti-VHH HRP. Each triplicate data point is shown, with a line connecting the mean. ELISA was conducted once.

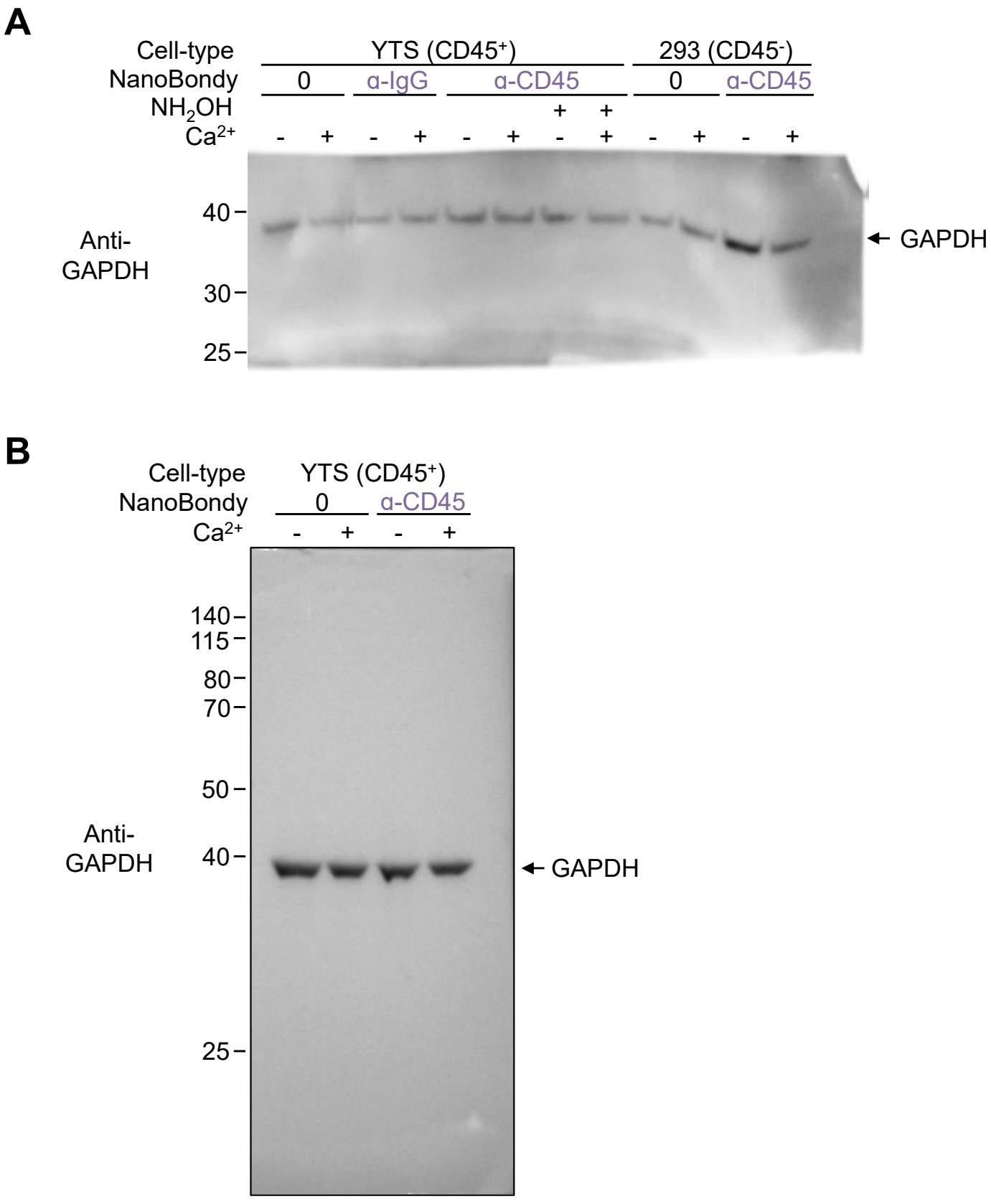

***Supplementary Figure 6*. Full-size GAPDH blots to accompany Figure 7. (A)** Western blotting of NanoBondy reaction. 5 μM anti-CD45 NanoBondy was incubated with YTS cells or Expi293F cells for 1 h at 37 ºC ± calcium. Western blot to glyceraldehyde-3-phosphate dehydrogenase (GAPDH) was used as the loading control. This section relates to Figure 7A. The membrane was cut in two pieces at the 50 kDa marker before blotting against GAPDH and the full membrane that was blotted is shown. Western blot was conducted once. **(B)** YTS cells were stained as in (A), except with 25 μM anti-CD45 NanoBondy. This section relates to Figure 7B. Western blot to GAPDH was used as the loading control. Western blot was conducted once.

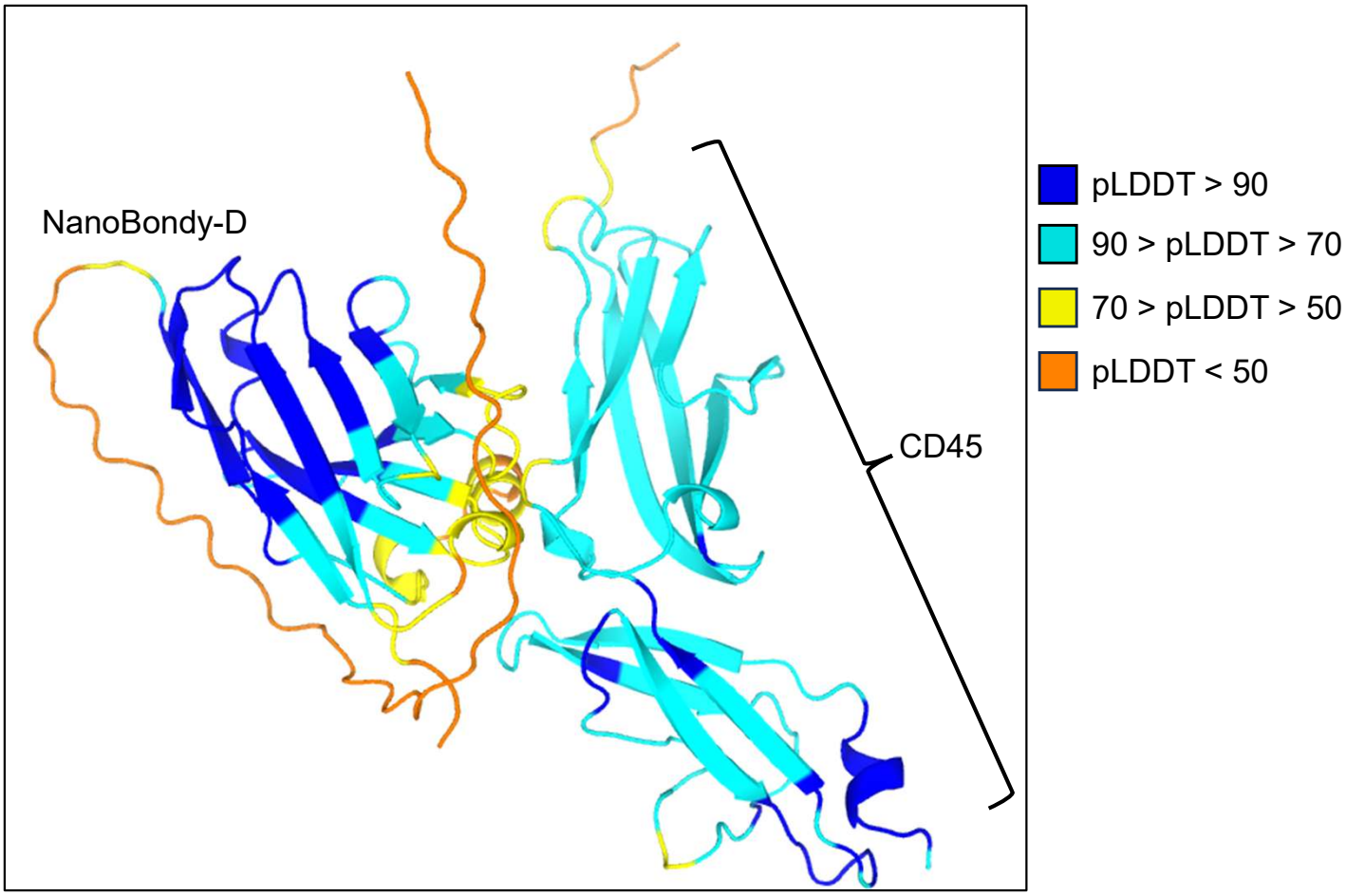

Supplementary Figure 7: AlphaFold2 prediction of NanoBondy/CD45d binding. AlphaFold2multimer prediction of 2H5 NanoBondy-D/CD45 structure, colored according to predicted Local Distance Difference Test (pLDDT) score. NanoBondy-D represents the NanoBondy following calcium-induced cleavage of the SPM.

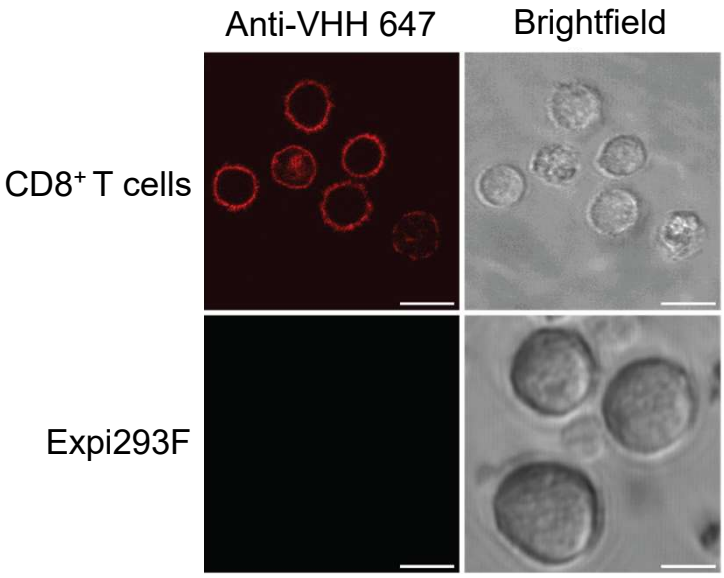

Supplementary Figure 8: Confocal microscopy of NanoBondy cell-surface labeling. Primary human $CD8^+$ T cells ($CD45^+$) or Expi293F cells ($CD45^-$) were incubated with 2 μM anti-CD45 NanoBondy for 1 hour at 25 ºC. NanoBondy was detected using anti-VHH-Alexa Fluor 647 (shown in red, left column) with brightfield image shown alongside (grayscale, right column). Images shown are confocal slices. Scale bar is 10 μm. Microscopy experiment was conducted once.